ACS OMEGA

Open Access

http://pubs.acs.org/journal/acsodf

Review

Main Control Factors of Fracture Propagation in Reservoir: A Review

Geng Liu, Changcheng Han,* Huijie Yang, Jinlei Xiu, Xin Li, Zhiwei Hao, Bo Wei,* and Ning Lv

Cite This: *ACS Omega* 2024, 9, 117−136

Read Online

ACCESS | Metrics & More | Article Recommendations

ABSTRACT: The fracture distribution and internal control factors after the fracturing of unconventional oil and gas reservoirs determine the reservoir reforming effect to a large extent. Based on the research of global scholars on the influencing factors of fracture propagation, comprehensive theoretical model, and numerical simulation, this Review systematically discusses the influence of internal geological factors and external engineering factors of unconventional oil and gas reservoir on fracture propagation behavior and summarizes the current problems and development trends in fracture research. The results show the following: (1) The fracture propagation is a comprehensive process constrained by lithology and mineral composition, water saturation, non-homogeneity, natural weak surface, and ground stress. (2) External engineering factors have a meaningful control effect on fracture propagation; the type and temperature of fracturing fluids can also change the mechanical properties of different rocks, thus affecting the fracture propagation pattern. (3) The existing fracture propagation models have certain limitations, and their computational reliability still needs to be further verified. (4) Numerical simulation can break through the limitations of physical simulation, but different simulation methods have different shortcomings and applicability. In the future, we should focus on: (1) finding parameters to quantitatively characterize heterogeneity at the 3D level, which is an important direction to study the effect of heterogeneity on fracture propagation; (2) introducing computerized methods to establish a geological model that considers multiple factors and combining it with numerical simulation software to study fracture propagation; (3) considering the characteristics of fluid−liquid−solid phase comprehensively, establishing a suitable THL coupling equation; (4) how the interaction mode of fracturing fracture is combined with the natural fracture geometry, and how the fracture is affected by fracturing engineering parameters such as fluid injection rate and viscosity of fracturing fluid; and (5) geology-engineering dynamic integration, which is an important direction to be carried out in the future.

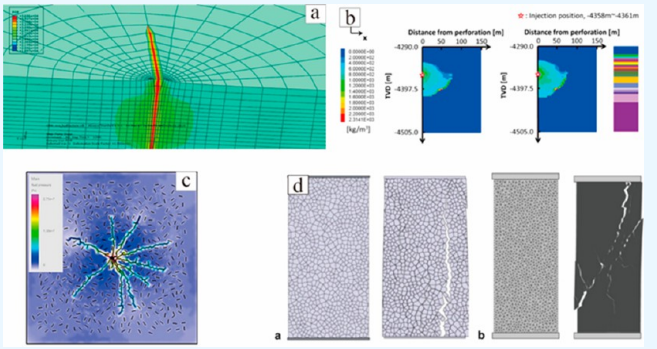

1. INTRODUCTION

With the further development of unconventional oil and gas resources, the demand for fracturing is gradually increasing.[1−3] Since 1947, when fracturing technology was first applied to oil and gas development, its favorable production effect has been widely studied.[4,5] There are many types of unconventional reservoirs, such as shale, coal, sandstone, etc., with different lithology, mineral composition, and heterogeneity; these factors will lead to irregular and distorted fracture propagation along the path, which will increase the risk of sand plugging.[6−8] The influence of water saturation on rock mechanical properties is mostly focused on the study of rock compressive (tensile) strength, shear, and creep properties, and the stress change caused by water content will also affect the expansion of fracturing fractures.[2,9,10] Natural fractures have dual functions of trapping and blocking fracture, which greatly increases the complexity of fracture propagation.[11,12] In situ reservoir pressure, reservoir thickness, and interlayer interfaces will control the length, height, width, and morphology of the fractures.[13,14] There is a lack of relevant research and systematic discussion on the quantitative evaluation of the influence of various geological factors on fracture propagation, indicating a need for further investigation.

Traditional hydraulic fracturing techniques use water-based fracturing fluids, which are widely applied due to their excellent ability to create fractures and sand carry proppants.[15,16] However, they have drawbacks such as incomplete backflow, large underground retention volume, groundwater contamination, high water consumption, and severe damage to formation.[17,18] Therefore, many new types of waterless fracturing technologies have emerged, among which CO_2 fracturing is more environmentally friendly, as it can save water resources, increase production, and achieve carbon

Received: November 1, 2023
Revised: December 6, 2023
Accepted: December 11, 2023
Published: December 28, 2023

sequestration.[19−22] Furthermore, different types of fracturing fluids have different physical properties, and there is relatively little research on their influence on fracture propagation. Previous studies have focused more on the mechanical parameters of rocks under high temperature and high pressure, and rarely consider their impact on rock fracturing behavior and fracturing fluid physical properties.[23,24]

Numerical simulation is an important tool for studying fracture propagation.[25−27] With the development of oil and gas exploitation, researchers have established typical models such as KGD and PKN to simulate fracture propagation. However, fracture propagation is a nonlinear and multifactor coupled boundary movement problem. Therefore, a series of numerical simulation methods for fracture propagation have emerged, including the finite element method (FEM), extended finite element method (XFEM), boundary element method (BEM), discrete element method (DEM), and finite-discrete combination method (FDEM).[28−31] Numerical simulation has been widely used to study geological and engineering factors such as in situ stress, proppant content, fracturing fluid viscosity, and flow rate. However, these studies have certain limitations, such as limited research in nonuniform stress fields, hydraulic fracture propagation laws, and fracture morphology.

Therefore, based on previous research achievements, this Review systematically analyzes the influence of geological and engineering factors on fracture propagation behavior. It provides a systematic review of the basic models and numerical simulation of fractures in unconventional reservoirs. This Review also proposes future research priorities and development directions, aiming to provide references for improving the level of fracturing technology.

2. THE INFLUENCE OF GEOLOGICAL FACTORS ON FRACTURE PROPAGATION

2.1. Lithology and Mineral Composition. The essence of formation rock fracturing is the deformation of rocks when their strength is lower than the circumferential stress they experience.[32] As the foundation of reservoir modification, different lithology has different mineral compositions, leading to different responses in the initiation and propagation of fractures.[33,34] For instance, softer rocks are more prone to forming wide fractures, while harder rocks are likely to form confined fractures.[32,35,36] Hou et al. conducted hydraulic fracturing on shale, limestone, and tight sandstone (Figure 1). The study showed that shale had the highest number of fractures and the most complex fracture propagation, forming a network of fractures with a large surface area. Although no fracture network was formed in limestone, the volume of the reservoir after the modification was significant. However, tight sandstone exhibited low levels of fracturing with few fractures, the simplest propagation pattern, and unsatisfactory modification effects (Table 1).[37]

The compressibility of reservoirs can be characterized by rock mechanical parameters, including Young's modulus, Poisson's ratio, tensile strength, fracture toughness, hardness, and brittleness index. Compressibility evaluation is primarily applied to shale reservoirs, with fewer applications in other unconventional reservoirs.[38−41] These rock mechanical parameters typically have a substantial influence on fracture propagation, with the brittleness index being the most important. It can determine the morphology and connectivity of fracture networks and is an important factor in fracture generation, network morphology, and the effectiveness of

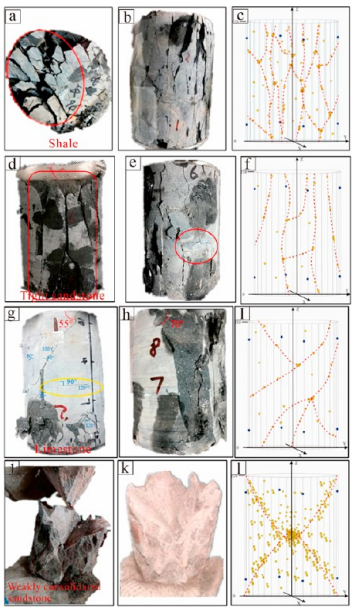

Figure 1. Actual fracture morphology and acoustic emission location map of fracturing with different lithology ((a,b,d,e,g,h,j,k) are the experimental result graphs, and (c,f,i,l) is the setting-out plan). Reprinted with permission from ref 36. Copyright 2021 Elsevier B.V.

fracturing in heterogeneous reservoirs.[42,43] Currently, there are many methods for quantitatively characterizing the brittleness index (Table 2), with BI_{20} and BI_{21} being the mainstream approaches. Evaluating brittleness based on rock mineral content is widely recognized as a reliable method.[44] Chen et al. categorized fracture patterns into simple shear fractures, simple fractures, X-shear fractures, and network fractures. Their research found that rocks with high brittleness mineral content are more likely to form X-shear and network fracture patterns, while rocks with low brittleness mineral content are more prone to form simple shear fracture patterns.[36] Young's modulus and Poisson's ratio have a significant impact on the fracture width and total fracture area, showing a positive correlation with the fracture height.[36,45−47] The mineral type influences the magnitudes of Young's modulus and Poisson's ratio. The correlation between Poisson's ratio and quartz and pyrite is the strongest. Pyrite and quartz have a higher Young's modulus and a lower Poisson's ratio, indicating good compressibility. Otherwise, clay, calcite, and dolomite have a lower Young's modulus and a higher Poisson's ratio, indicating poorer brittleness.[48,49] Fracture toughness and tensile strength can reflect the sensitivity of rocks to fracturing. Additionally, there is a linear correlation between rock tensile strength and fracture toughness. In the fracturing process, a higher fracture toughness indicates a greater likelihood of plastic deformation, resulting in higher initiation and propagation pressures.[40,41,50−53] Therefore, comprehensive analysis and evaluation of the lithological characteristics of the rock during fracturing can help optimize fracturing design and predict fracture propagation behavior, effectively improving production capacity and economic benefits.

2.2. Water Saturation of Rock. Previous researchers divided the stress−strain curve of rocks into five stages: stage I, crack closure; stage II, linear elastic deformation; stage III, stable crack propagation; stage IV, unstable crack propagation; and stage V, post-peak failure. They defined the stress points at the boundaries of each stage as follows: crack closure stress σ_{cc},

https://doi.org/10.1021/acsomega.3c08547
ACS Omega 2024, 9, 117−136

Table 1. Contrast of the Main Control Factors of Fracture Type[36]

	network fracture	simple fracture	simple shear fracture	X-shear fracture
brittle mineral (%)	>45%	35−45%	<35%	>45%
brittleness index	>0.42	>0.4	<0.32	>0.42
fracture pressure (MPa)	<65	<70	>70	<65
porosity (%)	>2.0%	1.5−2.0%	<1.0%	>2.0%
Young modulus (GPa)	<35	<35	>50	<30
principal stress difference (MPa)	<40	<40	>50	<35
interlayer modulus (GPa)	<3	<3	>3	<3
fracture network	more complicated	complicated	not complicated	more complicated
sample	shale or sandstone−mudstone interbedded rock	tight sandstone or sandstone−mudstone interbedded rock with parallel bedding under axial compression	limestone or sandstone−mudstone− limestone interbedded rock	weakly consolidated sandstone or coal
fracture treatment	best	better	poor	best

Table 2. Summary of Current *BI* Definitions[54,55]

formula	method and basis	method description or variable description
$BI_1 = \varepsilon_{II} \times 100\%$	based on loading and unloading tests	ε_{II} is the irrecoverable axial strain[56]
$BI_2 = \frac{H_\mu - H}{K}$	based on hardness experiments	H is microhardness, H_μ is microhardness, and K is permeability[57]
$BI_3 = q\sigma_c$	based on debris content	q is the percentage of debris with a particle size less than 0.60 mm, and σ_c is tensile strength[58]
$BI_4 = S_{20}$		S_{20} is the percentage of debris with a particle size less than 11.2 mm[59]
$BI_{11} = HE/K_{IC}^2$	based on hardness experiments	H is hardness, E is Young's modulus (MPa), and K_{IC} is breaking tenacity (MPa $m^{1/2}$)[59]
$BI_5 = H/K_{IC}$	based on hardness experiments	H is hardness, and K_{IC} is breaking tenacity (MPa $m^{1/2}$)[60]
$BI_6 = \varepsilon_r/\varepsilon_t$	based on loading and unloading tests	ε_r is recoverable strain, and ε_t is total strain[60]
$BI_7 = \sigma_C/\sigma_T$	based on strength characteristics	σ_C is uniaxial compressive strength, and σ_T is tensile strength[60]
$BI_8 = \sin\varphi$	based on internal friction angle	φ is the angle of internal friction corresponding to 0 on the Mohr's envelope[60]
$BI_9 = 45 + \varphi/2$		φ is the angle of internal friction between the damage surface and the surface of maximum principal stress action[60]
$BI_{10} = (\tau_p - \tau_r)/\tau_p$	based on full stress−strain curve	the functional relationship between peak stress intensity and residual stress intensity[61]
$BI_{12} = -1.8748 \times Ø + 0.9679$	based on logging data and laboratory measurements	Ø is porosity[51,62]
$BI_{13} = \frac{F_{max}}{P}$	based on penetration tests	ratio of load F_{max} to penetration depth P[63]
$BI_{14} = \frac{E_n + \nu_n}{2}$	based on full stress−strain curve	Young's modulus and Poisson's ratio normalized to the mean value[64]
$BI_{15} = \frac{E}{\nu}$		
$BI_{16} = \frac{E\rho}{\nu}$		ρ is density[65,66]
$BI_{17} = \frac{M - E}{M}$		E is unloading elastic modulus, and M is postpeak elastic modulus[67]
$BI_{18} = \frac{E}{M}$		M is constant[67−69]
$BI_{19} = \frac{E}{\lambda + 2\mu}$		
$BI_{20} = \frac{E}{\lambda}$		
$BI_{21} = \frac{Q}{Q + C + Cl}$	based on logging data or XRD	Q is quartz, C is carbonate mineral, and Cl is clay[44]
$BI_{22} = \frac{Q + Dol}{Q + Dol + Lm + Cl + TOC}$		Dol is dolomite, Lm is limestone, and TOC is total organic matter[70]

https://doi.org/10.1021/acsomega.3c08547
ACS Omega 2024, 9, 117−136

Table 3. Summary of Relationships between Water Saturation and Rock Mechanics Parameters

rock type	experimental method	variation of rock mechanical parameters
coal	uniaxial compression test	the uniaxial compressive strength and elastic modulus of rock decrease with the increase of water saturation[82]
argillaceous sandstone	uniaxial compression test, Brazil test	uniaxial compressive strength, elastic modulus, and tensile strength decrease with the increase of water saturation[83]
sandstone	uniaxial compression test	water saturation decreases, while rock stiffness and strength increase[84,85]
coal	uniaxial compression test	σ_{ci}/σ_{ucs} and σ_{cd}/σ_{ucs} decrease with the increase of water content[86]
coal	uniaxial compression test	the elastic modulus increases significantly with the decrease of water saturation[87]
sandstone	uniaxial compression test	the peak stress, elastic modulus, and brittleness index decreased with the increase of water saturation[9]
sandstone	triaxial compression test	the elastic modulus, peak strength, and residual strength decrease with the increase of water saturation[88]
red sandstone	uniaxial compression test	σ_{cd}/σ_{ucs} increases in the low water content state compared to the saturated state[35]
granite	triaxial compression test	tensile strength and compressive strength decrease with the increase of water saturation, while elastic modulus and Poisson's ratio have little change[79]

initiation pressure σ_{ci}, damage pressure σ_{cd}, and ultimate compressive strength σ_{ucs}.[71−74] Zhao et al. conducted a study on stress−strain curves and acoustic emission characteristics under different water saturation levels, indicating that water saturation primarily influences stages III, IV, and V, while its impact on the first two stages is relatively minor. This is attributed to the inhibitory effects of pore water pressure within microfracture and the Stefan effect on microcrack propagation.[35] The impact of water saturation on fracturing crack propagation is manifested as follows:

(1) An increase in water saturation alters the mechanical properties within the rock (Table 3). The presence of water molecules forms a lubricating layer around the fracture, reducing friction between rock particles, which leads to reduced cohesive forces within the rock, making fracture propagate more easily. Additionally, the presence of water increases the pore water pressure in the rock, making it more prone to fracturing and deformation. Typically, mechanical properties and rock strength exhibit exponential or power-law relationships with water saturation.[10,75] (2) At low water saturation levels, rocks tend to exhibit brittle and shear failure after peak strength. As water saturation increases, plastic failure becomes predominant. For rocks with high clay content, a reduction in moisture content can lead to increased stiffness and strength.[9] (3) Generally, the elastic modulus degrades with increasing moisture content, and Poisson's ratio increases. This is because water typically hinders stress within the rock, resulting in reduced overall stiffness and deformation capacity. However, some studies have shown that dry samples may exhibit more pronounced pore crack shrinkage, so Young's modulus of wet samples may be higher than that of dry samples during the initial compression stage.[75−77] (4) Sedimentary rocks are more sensitive to water as compared to igneous and metamorphic rocks. Previous research has indicated that water saturation has a smaller impact on the compressive and tensile strength of granite, with minimal effects on elastic modulus and Poisson's ratio. However, saturated conditions may reduce rock fracturing pressure, attributed to a decrease in Type I fracture toughness and the influence of water pressure within microcracks, which promotes fracture initiation.[78,79] (5) Increasing water saturation can enhance rock permeability, facilitating the transmission and expansion of fracturing fluid within the rock, promoting the fracture propagation. However, excessively high-water saturation in rock zones can increase fluid resistance, limiting fracture expansion.[79−81]

In summary, water saturation has a complex impact on fracture propagation, capable of altering the fracture propagation rate and mode. This effect is dependent on various factors, including rock type, water saturation level, and operational conditions. Therefore, in related engineering and research endeavors, it is essential to thoroughly consider the influence of water saturation on rock behavior.

2.3. Rock Heterogeneity. Heterogeneity within rocks is a widely existing characteristic, manifested by various physical, chemical, and structural features within the rock. Different shapes, strengths, and distributions of blocks within reservoirs can result in strong heterogeneity.[89,90] However, due to the difficulty of studying heterogeneity and its impact on fracture propagation in laboratory settings, numerical simulations are often relied upon.[7,47]

Heterogeneity significantly affects stress distribution around fractures, leading to the deflection of artificial fracture paths. As the fracture propagates from a soft rock layer to a hard rock layer, the fracture undergoes obvious deflection. In contrast, when the fracture propagates from a hard rock layer to a soft rock layer, the deflection is less obvious. This indicates that the presence of hard blocks changes the path of fracture propagation and increases the complexity of fracture expansion. Additionally, the local distribution of hard or irregular blocks within a reservoir can cause the fracture to bend, altering its shape. This promotes fracture expansion in length but limits it in width.[14,26] The heterogeneous distribution of particles also affects the expansion of fractures. Huang et al. divided the interaction between fractures and particles into six types (Figure 2) and compared the expansion

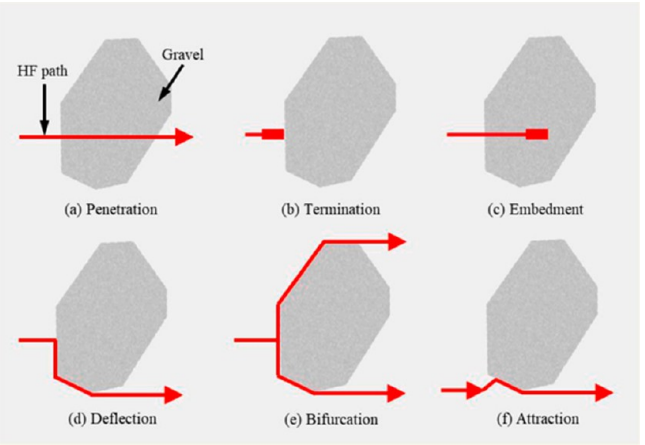

Figure 2. Schematic diagram of typical types of HF/G interaction: (a) penetration, (b) termination, (c) embedment, (d) deflection, (e) bifurcation, and (f) attraction. Reprinted with permission from ref 92. Copyright 2023 Elsevier B.V.

https://doi.org/10.1021/acsomega.3c08547
ACS Omega 2024, 9, 117−136

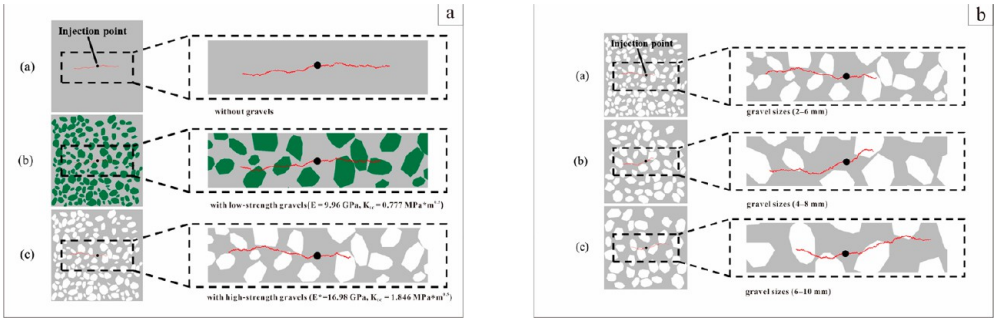

Figure 3. Comparison of fracture growth with different effective toughness and different particle size: (a) with different effective toughness and (b) with different particle size. Reprinted with permission from ref 92. Copyright 2023 Elsevier B.V.

characteristics of fractures in homogeneous and heterogeneous rocks with different particle sizes (Figure 3). The results showed that the effective toughness of rocks with heterogeneous particle distribution was 30% higher than that of homogeneous rock samples. Increasing the particle size increased the resistance to fracture propagation. Additionally, there was a positive correlation between the particle size and fractal dimension of rocks and their tensile strength and fracture toughness. Therefore, fractal dimension can be used as a quantitative descriptor of the heterogeneity of microscopic particle distribution within rock.[91−93] The elastic modulus of low-ductility minerals has a critical influence on the connectivity of fractures. The larger is the Young's modulus in a region, the easier it is for the fracture to propagate. Therefore, the heterogeneity of mineral composition affects the geometric shape, expansion direction, and distance of fractures.[94−97] Previous studies on heterogeneity did not consider the various propagation modes of fractures, such as toughness-dominated (TDR) and viscosity-dominated (VDR) modes. This is an important direction for future research on the impact of heterogeneity on fracture propagation. Due to the complexity of reservoir heterogeneity and fracture propagation, production forecasting has become more uncertain. Therefore, it is critical to consider the distortion of fracture paths, the diversity of fracture shapes, and the nonuniformity of fracture expansion rates. Advanced numerical simulation and monitoring techniques are needed for a more accurate analysis of fracture propagation, to maximize reservoir fracturing efficiency and productivity.

2.4. Natural Fracture Distribution. Various types of fractures naturally form in the formation, including open, closed noncemented, and closed cemented fractures. The interaction between artificial fractures and natural fractures can be simply summarized as crossing, opening, and expanding (Figure 4); these fractures provide pathways for the storage and transportation of petroleum. It is generally believed that artificial fractures intersecting with natural fractures either can pass through the natural fractures or are blocked by the expansion or shear displacement of the natural fractures. The

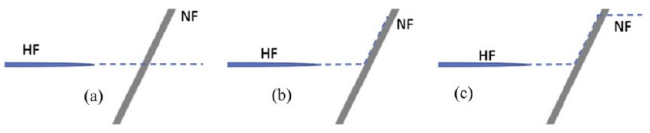

Figure 4. Intersection criterion between 2D fracture: (a) crossing, (b) opening, and (c) expanding. Reprinted with permission from ref 112. Copyright 2015 Elsevier B.V.

main behavior of fracture expansion is either creating a grid or passing through the grid. However, Wan et al. argue that conventional 2D intersection criteria cannot fully describe the geometry of hydraulic fractures. By studying the relationship between different-sized natural fractures and 3D hydraulic fractures (Figure 5), they classified the modes of fracture

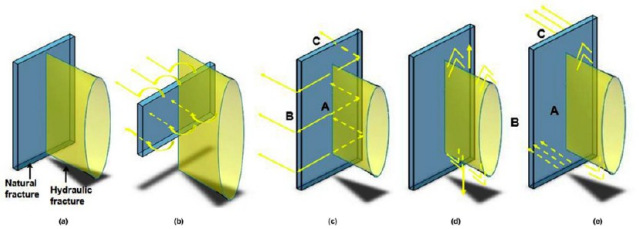

Figure 5. 3D fracture intersection criteria: (a) arresting, (b) bypassing, (c) diversion, (d) vertical extension, and (e) vertical extension and then diversion. Reprinted with permission from ref 98. Copyright 2018 Elsevier B.V.

propagation as arresting, bypassing, diversion, vertical extension, vertical extension, and then diversion.[98] Open fractures are generally more prone to hydraulic pressure expansion, while closed cemented fractures may present greater challenges. Researchers have also classified natural fractures into active and nonactive categories. Microseismic monitoring has indicated that nonactive natural fractures have no influence on the geometry of artificial fractures, while active natural fractures can alter the local stress direction by perturbing the stress field, thereby affecting the geometry of artificial fractures.[99]

The distribution of natural fracture systems plays a dual role in capturing and impeding the expansion of artificial fractures, which can limit the length of artificial fractures and exacerbate their nonuniform propagation. The presence of natural fractures increases the complexity of hydraulic fractures. (1) Due to the directional guidance effect of natural fractures on fracturing fluid and their interconnectivity, when the natural fracture density is low, a single dominant fracture with a larger length is mainly formed, resulting in a less complex fracture network. However, as the density of natural fractures increases, the length of artificial fractures decreases, and the complexity of the fracture network significantly increases, which is beneficial for enhancing reservoir stimulation.[31,34,100−102] (2) The dip angle of natural fractures influences the ability of artificial fractures to either intersect or bypass them. The angle between natural fractures and the direction of hydraulic fracture propagation is referred to as the approach angle, which

https://doi.org/10.1021/acsomega.3c08547
ACS Omega 2024, 9, 117−136

affects their intersection relationship. Artificial fractures can pass through natural fractures only when the approach angle is close to 60° or when there is a high horizontal differential stress. In cases of low horizontal differential stress or low approach angle, existing fractures may be reopened. Furthermore, artificial fractures can be blocked by the shear displacement of natural fractures only in cases of high differential stress and approach angles of 30−60°.[103−105] Zheng et al. divided the area into three regions based on the approach angle and stress differential (Figure 6). In the

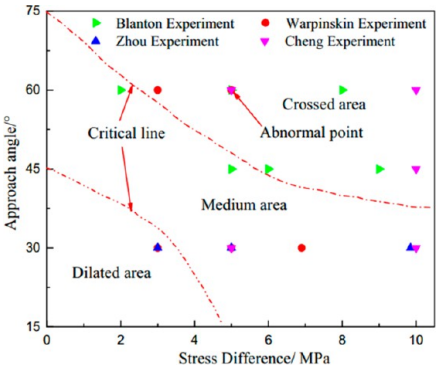

Figure 6. Natural fracture and stress difference and approach angle. Reprinted with permission from ref 113. Copyright 2020 Elsevier B.V.

expansion region, hydraulic fractures are easily intercepted by natural fractures, resulting in branching and extension along natural fractures. In the middle region, upper branches of natural fractures are reactivated, and artificial fractures propagate along natural fractures. In the intersection region, natural fractures are not reactivated.[106] (3) The cementation degree of natural fractures determines whether hydraulic fractures can cross them. A smaller cementation thickness makes it easier for artificial fractures to penetrate cemented natural fractures, resulting in longer artificial fractures and less complex fracture networks. As the cementation thickness increases, the rock−fracture interface weakens, making it more likely for artificial fractures to divert into cemented natural fractures. This results in shorter hydraulic fractures and more complex fracture networks.[104,107−109] (4) The fractal dimension of natural fractures is a crucial parameter for characterizing the distribution of fractures. As the fractal dimension increases, the number of natural fractures opened and connected by artificial fractures increases. Simultaneously, the maximum width of fractures decreases, and the number of fracture propagation directions increases, ultimately leading to the formation of a complex network of fractures.[110] Due to these factors, the detection of natural fractures becomes particularly important, and various methods for detecting fractures at different scales have been summarized[111] (Figure 7).

In conclusion, the impact of natural fractures on artificial fracture propagation is a complex and multifaceted issue that requires comprehensive consideration of fracture types, densities, orientations, cementation degrees, etc. In depth understanding and acquisition of actual data are crucial for studying fracturing strategies.

2.5. Formation Thickness and Interlayer Interface. Due to the influence of depositional processes, unconventional oil and gas reservoirs often exhibit multiple layers with different mechanical properties, and these interfaces are

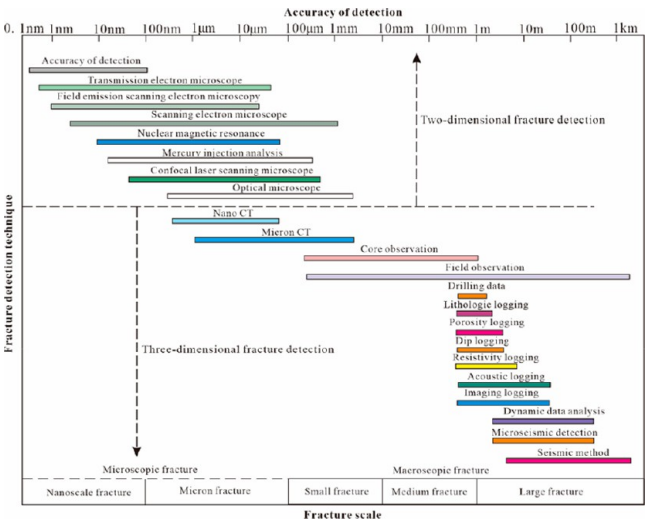

Figure 7. Different scale crack identification.

different from interbedded lithological interfaces, typically possessing higher cohesive strength (Zou et al., 2020). When an artificial fracture encounters a horizontal or inclined formation interface, the fracture may stall and propagate along the interface, leading to an increase in fracture length. Conversely, if the formation interface is perpendicular to the propagation direction of the artificial fracture, the height of the fracture may be constrained by the interface. The three main interaction modes between artificial fractures and bedding planes are similar to the intersecting criteria of 2D fractures (Figure 8): (1) fractures crossing the plane; (2) fractures

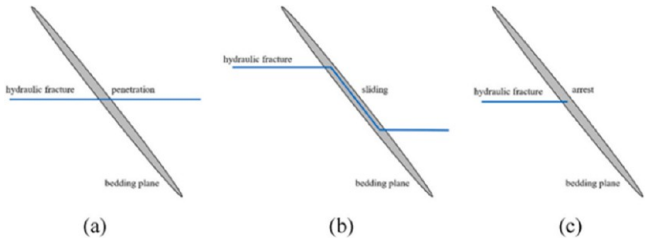

Figure 8. Interaction modes of three types of fractures with bedding planes: (a) fractures crossing the plane; (b) fractures slipping and crossing afterward; and (c) fractures being trapped by the bedding plane. Reprinted with permission from ref 114. Copyright 2017 Elsevier B.V.

slipping and crossing afterward; and (3) fractures being trapped by the bedding plane. Subsequently, researchers have further enriched this understanding (Figure 9).[13,14,114,115]

There exists a competitive relationship between rock strength and interbedded interface strength. When the interbedded interfaces are weakly cemented and have lower strength than the rock's fracture strength, the fracture pressure is relatively low. Conversely, when the interbedded interfaces are well-cemented and have higher strength than the rock's fracture strength, the fracture pressure is relatively high.[32,116] An increase in interface strength can result in an increase in fracture height (Figure 10) and a decrease in fracture width. Additionally, formation interfaces may influence the connectivity between multiple fractures, with connections to other fractures increasing the effective permeability of the reservoir. The geometric shape of the interface is also important, as

https://doi.org/10.1021/acsomega.3c08547
ACS Omega 2024, 9, 117−136

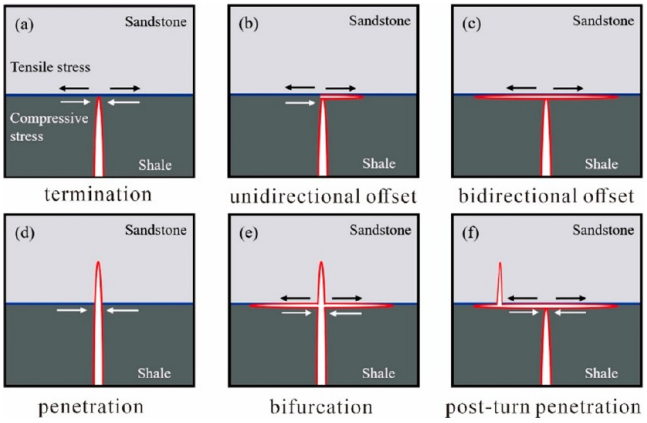

Figure 9. Interaction modes between fracture and interface: (a) termination, (b) unidirectional, (c) bidirectional offset, (d) penetration, (e) bifurcation, and (f) post-turn penetration. Reprinted with permission from ref 123. Copyright 2023 Elsevier B.V.

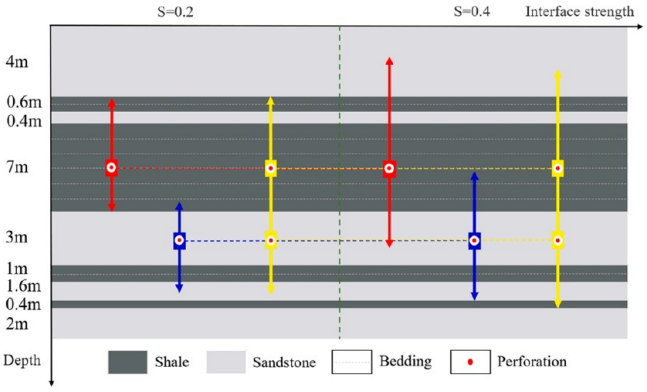

Figure 10. Fracture height under different perforating positions and maximum fracture penetration height when shale and sandstone are perforated simultaneously. Reprinted with permission from ref 123. Copyright 2023 Elsevier B.V.

interfaces of different shapes can have varying effects on the expansion path and propagation velocity of the fractures.

The key characteristic that differentiates shale reservoirs from other oil and gas reservoirs is the presence of weak bedding planes. The stiffness of bedding planes is typically measured using the ultrasonic method and the digital image correlation (DIC) method.[117,118] (1) The smaller is the stiffness of bedding planes, the greater is the shear slip displacement along the bedding planes. (2) With an increase in bedding plane density, the main fractures become connected to more bedding planes. However, excessive connectivity to bedding planes severely limits the extension of fractures in terms of length and height. (3) An increase in bedding plane strength corresponds to an increased difficulty in opening bedding planes and an increased possibility of artificial fractures propagating through the bedding planes.[119] (4) When there are numerous weak bedding planes, where the tensile strength of the bedding planes is lower than that of the matrix, a network of fractures may form. When the tensile strength of the bedding planes is lower than that of the matrix, the fractures propagate along the bedding planes. When they are comparable, the fractures do not fracture along the bedding planes.[37] (5) The permeability of the bedding planes influences the fracture propagation pattern. When the permeability of the bedding planes increases, fractures may be arrested and stop propagating. (6) Fracture termination is more likely to occur at weak bedding contacts and shallow burial depths. Fracture propagation through interfaces is possible when the interfaces are stronger and the burial depths are deeper.[108]

The influence of formation thickness on the propagation of fracturing fractures can be seen in the following aspects: (1) The thickness of the formation directly determines the distance over which fractures can propagate vertically and the shape of the fractures. In thinner formations, fractures are more easily propagated along simple paths due to less constraint, while in thicker formations, the propagation pattern of fractures becomes more complex. (2) The thickness of the formation also affects the distribution of pressure. In thinner formations, pressure may more easily establish within the fractures, thus promoting their propagation. In thicker formations, pressure may be more evenly distributed, requiring higher pressure to drive fracture propagation. (3) The thickness of the formation is often accompanied by changes in rock properties. The fracture toughness of the reservoir and interbeds reflects the ability of the rocks to resist instability and expansion. The fracture toughness of interbeds can restrict the growth of fracture penetration height. The length and width of fractures are positively correlated with the fracture toughness of the reservoir and interbeds. If the fracture toughness of the interbeds is sufficient, it can act as a barrier to prevent fractures from propagating in the vertical direction.[110] Developed natural weak structures such as bedding planes and joint planes are prerequisites for unconventional oil and gas reservoir volume enhancement. Especially in multilithology formations, the characteristics of interlayer weak planes vary greatly, leading to complex fracture morphologies after fracturing.[120−122] In practical engineering, detailed geological and engineering analysis must be conducted to understand the nature, location, geometric shape, and thickness of the formation interfaces, to better understand the propagation behavior of the artificial fractures.

2.6. Stress State. The impact of stress conditions on the expansion of fracturing fractures can mainly be discussed from three aspects: pore pressure, stress difference, and confining pressure. The existence of pore pressure can increase the permeability of reservoir or rocks, helping to drive the fracturing fluid into the deep rock. However, in some cases, a high pore pressure may cause compaction of the formation, inhibiting the expansion of fractures. Pore pressure can help maintain the stability of the fracturing fractures, counteracting some of the liquid pressure, thereby reducing the stress on the fracture walls and preventing fracture closure and collapse. Pore pressure is usually related to the pore structure and porosity in the reservoir, with higher porosity often leading to higher pore pressure, which can promote fracture expansion. However, when using a water-based medium as the fracturing fluid, it is difficult to effectively penetrate into the pores at a certain depth. Therefore, the fluid cannot form a high-pore pressure zone, which is the reason why the traditional hydraulic fracturing criteria neglect the influence of pore pressure. However, SC-CO_2 has extremely low viscosity and surface tension, and its penetration is very strong. The effect of pore pressure on fracturing pressure cannot be ignored.[77]

In the vertical expansion of fractures, the geometric shape and complexity of the fractures increase as the vertical stress difference decreases. With an increase in vertical stress, the formation interface undergoes compaction, resulting in a significant increase in resistance to fracture propagation along

https://doi.org/10.1021/acsomega.3c08547
ACS Omega 2024, 9, 117−136

the formation interface. This leads to an increase in initiation pressure and difficulty in fracturing along the formation interface. A smaller stress difference will result in a network of branching fractures, while a larger stress difference will form relatively simple fracture patterns (Figure 11). An increase in

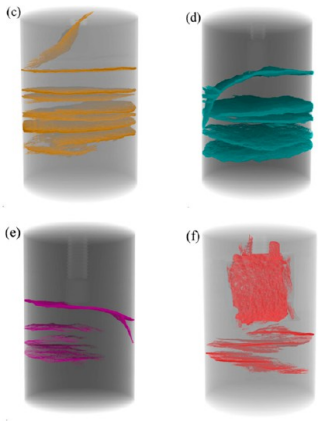

Figure 11. Fracture networks generated by different vertical stress differences: (c) σ_c and σ_a of 20 × 20, (d) 20 × 15, (e) 20 × 10, and (f) 10 × 20 MPa. Reprinted with permission from ref 63. Copyright 2021 ACS Publications.

vertical stress difference leads to an increase in the total height of the fractures (Figure 12).[34,63,113,123] However, if it is the stress difference between the reservoir and adjacent layers, the height of the fractures is negatively correlated with it; that is, the greater is the stress difference, the smaller is the fracture height. As the stress difference decreases, the closure pressure inhibiting fracture propagation decreases, resulting in an increase in net proppant pressure acting on the fracture walls, leading to an accelerated growth in fracture height. However, if the stress difference between the reservoir and adjacent layers is too large, the growth of fracture height will be controlled, and the energy of the fluid will be transmitted along the length and width of the fractures. When the horizontal stress difference is weak, fractures initiate along the weak planes around the simulated borehole and change direction toward natural fractures and bedding planes, without obvious transverse fractures. With an increase in horizontal stress difference, transverse fractures can be clearly observed, and the results of hydraulic fracturing and SC-CO_2 fracturing are more consistent (Figure 13).[48,123] The coefficient K_h is commonly used to characterize the stress difference in terms of the in situ stress.

$$K_h = \frac{\sigma_H - \sigma_h}{\sigma_h} \times 100\% \quad (1)$$

where σ_H is the maximum horizontal principal stress, and σ_h is the minimum horizontal principal stress.

Research has shown that both heterogeneous and homogeneous rock models exhibit a watershed in the fractal characteristics of fracture networks when the stress ratio σ_H/σ_h is 1.5. At a stress ratio of 1.5, the fractal dimension reaches its maximum value. When the stress ratio exceeds 1.5 and reaches 1.7, the fractal dimension rapidly decreases with increasing stress ratio, indicating a decrease in the development and complexity of the fracture network. A stress ratio of 1.7 may be the threshold at which a network composed of multiple fractures transitions to single-wing or double-wing fractures, suggesting that a larger stress difference leads to a smaller fractal dimension of the fracture network, making the occurrence of a single fracture more likely.[124]

The effect of confining pressure on fracture propagation is primarily characterized by a transition from longitudinal tensile failure to shear failure as the confining pressure increases. Confining pressure also hinders the initiation of fractures, with higher confining pressures requiring greater pressure to initiate fractures in the rock (Figure 14).[125]

In conclusion, factors such as pore pressure, stress difference, and confining pressure play a significant role in the fracturing process, affecting the pore structure of the rock, distribution of underground stress, fracture size, fracture stability, initiation pressure, and fracture propagation direction. These factors need to be carefully considered and managed during the hydraulic fracturing process.

3. ENGINEERING PARAMETER

3.1. Fracturing Fluid Type. Different fracturing fluids have distinct physical characteristics (Table 4). Water-based fracturing fluids play a crucial role in hydraulic fracturing. However, due to their significant water consumption, potential environmental impacts, and relatively poor fracturing performance, it has prompted the emergence and development of waterless fracturing techniques.[126,127] Variations in the composition and state of the fracturing fluid can lead to changes in the fracture path and initiation pressure. The type of fracturing fluid affects the initiation pressure, and when using SC-CO_2, the initiation pressure is 15% lower as compared to L-CO_2 and nearly 50% lower than that required for hydraulic fracturing (Figure 15).[77] Additionally, permeability serves as a direct indicator of reservoir enhancement. Therefore, the changes in permeability for hydraulic fracturing and SC-CO_2 fracturing have been summarized in Table 5. As

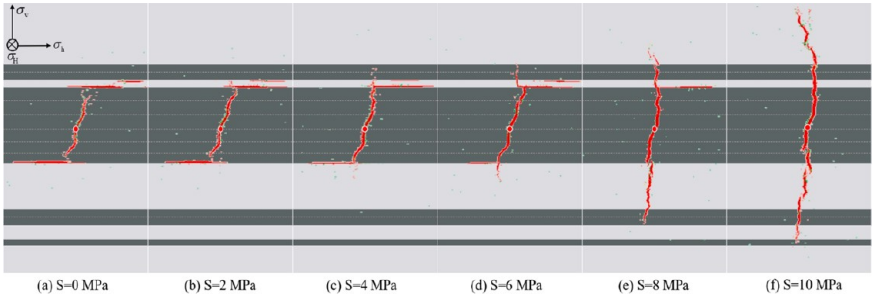

Figure 12. Results under different vertical stress difference: (a) S = 0 MPa, (b) S = 2 MPa, (c) S = 4 MPa, (d) S = 6 MPa, (e) S = 8 MPa, and (f) S = 10 MPa. Reprinted with permission from ref 123. Copyright 2023 Elsevier B.V.

https://doi.org/10.1021/acsomega.3c08547
ACS Omega 2024, 9, 117−136

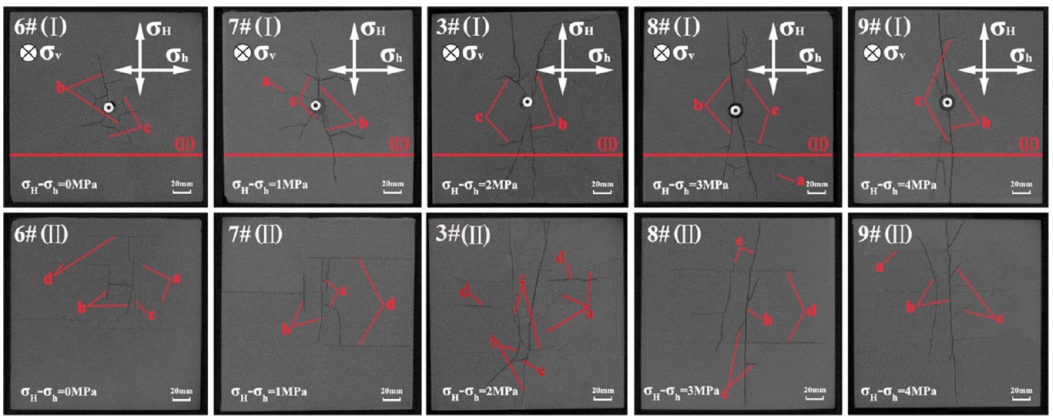

Figure 13. CT scanning images of shale specimens fractured under different horizontal stress differences with SC-CO_2 used as the fracturing medium: (6#) 0 MPa, (7#) 1 MPa, (3#) 2 MPa, (8#) 3 MPa, and (9#) 4 MPa. Reprinted with permission from ref 77. Copyright 2017 Elsevier B.V.

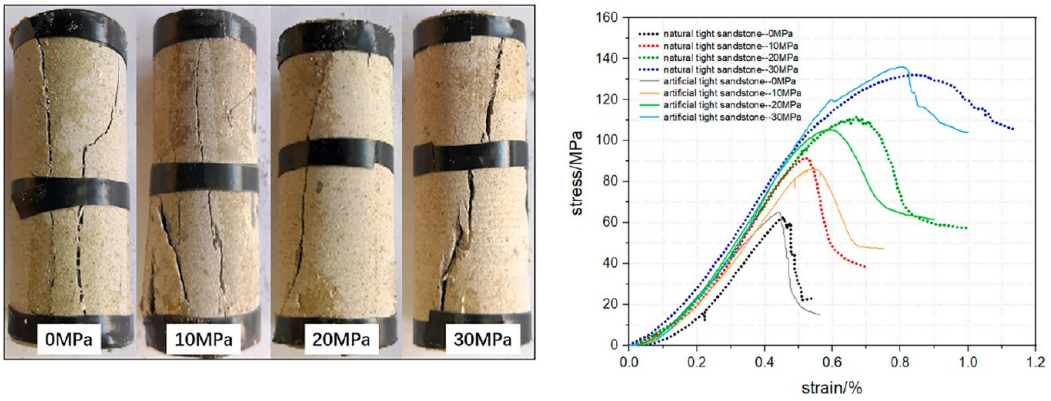

Figure 14. Fracture modes and stress−strain curves of artificial tight sandstone under different confining pressures: (a) fracture modes and (b) stress−strain curves. Reprinted with permission from ref 125. Copyright 2021 Elsevier B.V.

Table 4. Applicable Conditions and Limitations of Different Types of Fracturing Fluids[127]

type	application effects	limitations
water-based	low cost, suitable for large-scale use, and generating simple fractures[134]	large water consumption and the generation of a significant amount of wastewater may lead to regional seismicity, water lock reactions, and damage to formations[135]
air	prone to generating fracture branching and larger surface roughness[53]	poor carrying capacity of proppants[136]
LPG	no fluid loss, resulting in better effective fractures[136]	generates a large amount of flammable propane
N_2-based	can enhance the connectivity of pore and fracture networks, can quickly clean without impacting the environment, L-N_2 has a large compression coefficient and strong expansion ability, and has high elasticity[137−139]	poor carrying capacity of proppants, not suitable for use in plastic formations[140]
CO_2-based	good permeability, low viscosity, generates finer and more complex fracture networks, increases methane and hydrocarbon production, and favorable for carbon sequestration[77,141]	poor carrying capacity of proppants, leading to significant loss and leakage, strict requirements for fracturing equipment, preparation and transportation of carbon dioxide[31]

the viscosity of the fracturing fluid increases, the difficulty of crack propagation increases, resulting in an increase in fracture pressure and internal fracture aperture.[128] This leads to a decrease in fracture length but an increase in fracture width at the fracture mouth (Figure 16). Additionally, it is considered that the impact of fracturing fluid viscosity on hydraulic fracturing trajectory and fracture pressure can be neglected.[129] High viscosity fluids can prevent filtration, and reduce the likelihood of shale shear sliding and hydration expansion, thereby reducing fracture complexity. They also facilitate the vertical propagation of hydraulic fractures and allow them to cross multiple bedding planes.[113] However, low viscosity fluids experience less pressure drop along the bedding planes, have lower proppant-carrying capacity, and result in larger filtrate volume. This makes it easier to reach the initiation pressure at the end of the bedding planes, leading to the generation of complex and narrow fractures.[37] In comparison between L-CO_2 and water-based fracturing fluids (Figure 17), it is observed that after fracturing with L-CO_2, fractures tend to deviate and secondary branching fractures occur in the expansion direction. The degree of fracture bending is greater than in hydraulic fracturing, and the morphology of fractures tends to have a three-dimensional spatial distribution. The surface roughness of fractures is also greater.[130] The chemical composition of fracturing fluids can affect the dissolution and corrosion properties of rocks. Unlike water-based fracturing fluids, under high pressure, CO_2 can extract hydrocarbons from tight oil reservoir rocks, dissolve the rock matrix and minerals,

https://doi.org/10.1021/acsomega.3c08547
ACS Omega 2024, 9, 117−136

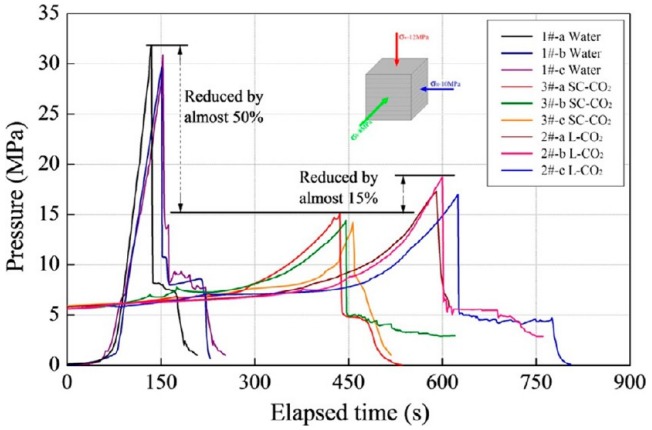

Figure 15. Variation of fracture initiation pressure with different fracturing fluids. Reprinted with permission ref 77. Copyright 2017 Elsevier B.V.

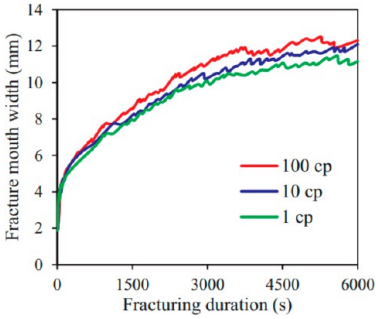

Figure 16. Fracture width changes with time under different fracturing fluid viscosity. Reprinted with permission from ref 129. Copyright 2019 Elsevier B.V.

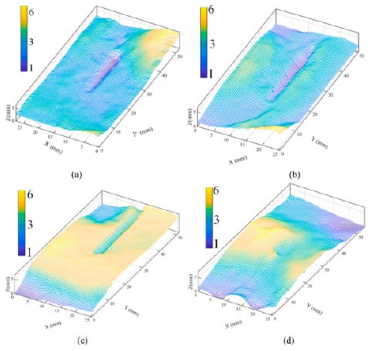

Figure 17. Comparison of water-based and L-CO_2 fracturing fluid numerical simulation. Reprinted with permission from ref 144. Copyright 2021 Elsevier B.V.

and migrate, which can effectively alter the pore structure[131] (Figure 18). SC-CO_2 has a much lower viscosity than water-based fracturing fluids, and its surface tension is close to zero, resulting in a much higher permeability as compared to water-based fluids. During the fracturing process, SC-CO_2 is more capable of penetrating through disconnected micropores in rock, transmitting fluid pressure to the deep parts of the rock, and forming a high-pore pressure zone around the wellbore. The increase in pore pressure can reduce the effective stress around the wellbore, lower the rock strength, and make it more prone to fracturing, inducing microfractures. The resulting fracture network is more complex as compared to water-based fracturing fluids (Figures 19 and 20).[77,123,132,133]

In general, different formations and production targets require different types of fracturing fluids. The optimization of fracturing fluid formulations is achieved through laboratory testing and numerical simulations, to achieve the best conditions for controlling and expanding fractures.

3.2. Temperature and Injection Pressure. Fracturing is a multiphysics coupling problem involving three physical processes (Figure 21): (1) initiation and propagation of high-pressure induced fractures, (2) heat conduction and transfer between the fracturing fluid and rock, and (3) fluid flow between fracturing fluid and rock matrix. Fracturing occurs when the pressure exceeds the rock fracture pressure and continues to propagate when the pressure exceeds the extension pressure.[145,146]

Temperature can alter the physical properties of rocks, and the mechanical properties of different rocks change differently with temperature variations[23] (Figure 22). For example, in sandstone, as the temperature increases, the fracture toughness of the rock decreases, leading to a decrease in both initiation and fracture pressures. Numerical simulations indicate that when the temperature rises to 200 °C, there is a significant change in the geometric shape of fractures, with fractures crossing bedding planes and causing some damage to the bedding planes. Consequently, both fracture and extension pressures decrease (Figure 23), increasing the possibility of fracture initiation and propagation. In carbonate rocks, as the temperature increases, the velocity of sound decreases, the compressive strength and axial strain increase, and the elastic modulus decreases.[24] In shale, as the temperature increases, the compressive strength and elastic modulus initially increase and then decrease, while the axial strain gradually increases until it reaches a maximum.[79,147]

An increase in temperature will also reduce the viscosity of the fracturing fluid, meaning that fracturing fluids are more likely to flow under high-temperature conditions. This effect is particularly significant in the case of CO_2 fracturing. The temperature and pressure variations during CO_2 fracturing can result in complex phase changes. Initially, CO_2 is stored in a liquid state, and as CO_2 is injected, temperature and pressure increase. When the temperature reaches 304.25 K and the pressure reaches 7.38 MPa, CO_2 enters a supercritical state. The SC-CO_2 fluid exhibits several distinct characteristics from CO_2, including low viscosity, zero surface tension, and high

Table 5. Effect of Fracturing Fluid on Permeability

fracturing fluid	rock type	prefracture permeability	permeability after fracturing	permeability variation
water-based	shale	$\sim 10^{-9}$ um^2	$\sim 10^{-7}$ um^2	increase of 2 orders of magnitude[134]
	coal	$(10^{-6}-10^{-7})$ um^2	$\sim 10^{-5}$ um^2	improvement of 1−2 orders of magnitude[142]
Sc-CO_2	shale	$(0.068-0.393) \times 10^{-6}$ um^2	$(0.732-1.520) \times 10^{-3}$ um^2	improved by 3−4 orders of magnitude[143]
	shale	$\sim 10^{-9}$ um^2	$\sim 10^{-4}$ um^2	improved by 4−5 orders of magnitude[134]
	coal	$(10^{-6}-10^{-7})$ um^2	$\sim 10^{-4}$ um^2	improved by 2−3 orders of magnitude[142]

https://doi.org/10.1021/acsomega.3c08547
ACS Omega 2024, 9, 117−136

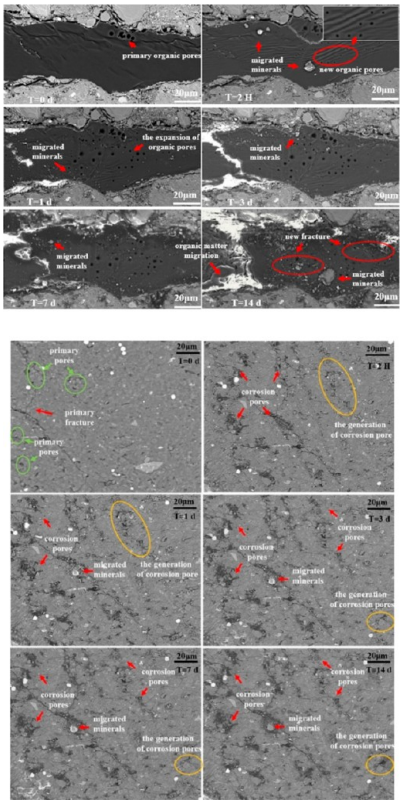

Figure 18. SEM analysis of CO_2 infiltration into organic matter in rock indicates that, with increasing infiltration time, CO_2 can generate more etching pores within the organic matter and cause mineral migration. Reprinted with permission from ref 131. Copyright 2021 ACS Publications.

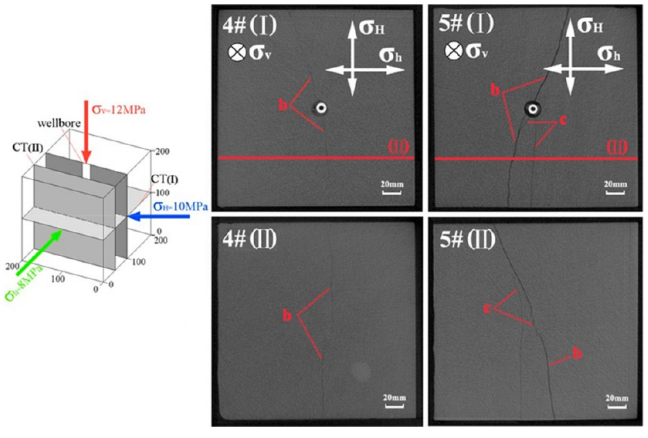

Figure 19. CT scanning images of sandstone specimens: (4#) water-based and (5#) SC-CO_2. Reprinted with permission from ref 77. Copyright 2017 Elsevier B.V.

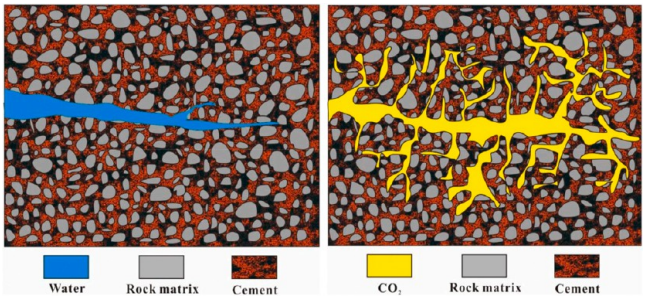

Figure 20. Schematic diagram of rock fractured by different fracturing fluids. Reprinted with permission from ref 132. Copyright 2021 Elsevier B.V.

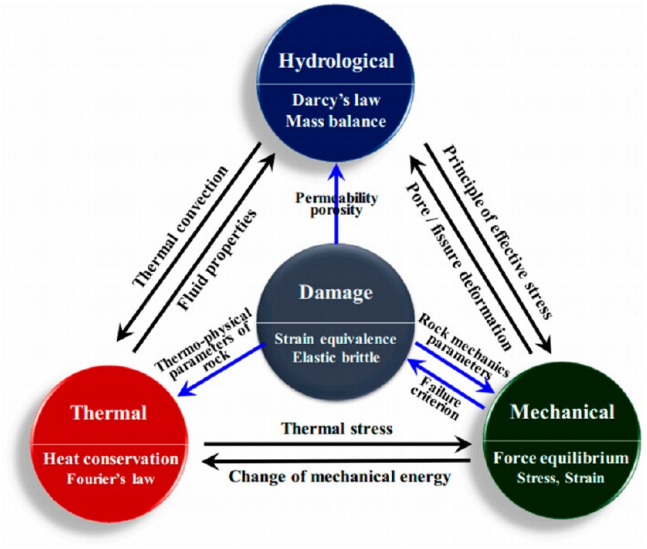

Figure 21. Schematic diagram of the THM coupling model. Reprinted with permission from ref 145. Copyright 2023 Elsevier B.V.

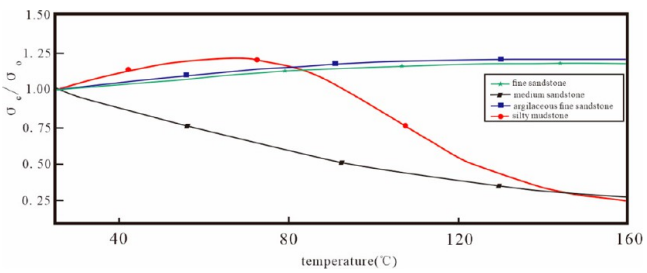

Figure 22. Influence of temperature on the compressive strength of different lithologies. Reprinted with permission from ref 23. Copyright 2017 Elsevier B.V.

diffusion coefficient.[28,123] Under high-temperature conditions, the density and viscosity of SC-CO_2 are less influenced by pressure, and it remains in a high-density, low-viscosity state (Figure 24).[77,109,133] After CO_2 enters the reservoir, it flows into the formation under injection pressure, and during diffusion, the pressure gradually decreases, approaching the formation pressure. Upon flowback, some CO_2 flows from the wellbore to the surface, causing a rapid decrease in CO_2 pressure, at which point CO_2 exists in a gaseous state. Temperature and pressure variations result in significant changes in fluid properties, further complicating the fracturing mechanism (Figure 25).[148−151]

The injection pressure also directly affects the reservoir pore pressure, distribution of minimum principal stress, and propagation behavior of the fracturing cracks. The greater is the injection pressure, the smaller is the effective minimum principal stress around the fracture tip, resulting in a larger deviation angle of the fracturing fracture. The formula is as follows:[129]

$$\theta_d = 0.8854P_w - 12.646 \quad (2)$$

https://doi.org/10.1021/acsomega.3c08547
ACS Omega 2024, 9, 117−136

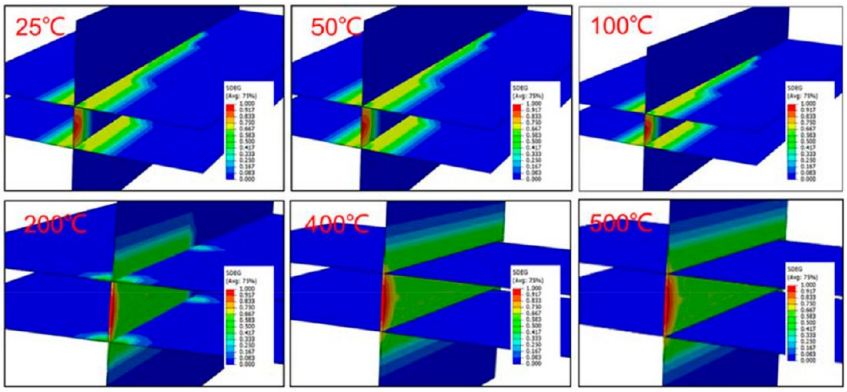

Figure 23. Fracture geometry under different temperature. Reprinted with permission from ref 14. Copyright 2021 Elsevier B.V.

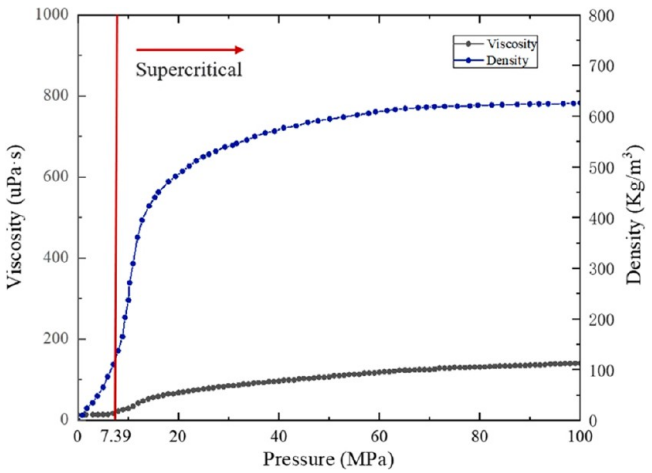

Figure 24. Density and viscosity change of CO_2 with pressure at 348 K. Reprinted with permission from ref 123. Copyright 2023 Elsevier B.V.

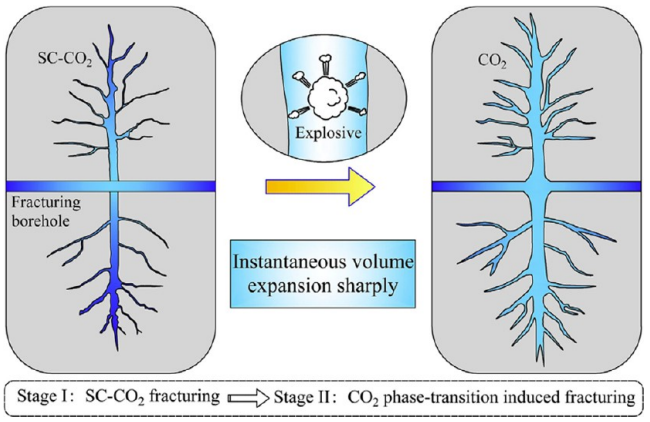

Figure 25. SC-CO_2 fracturing and CO_2 phase change fracturing model diagram. Reprinted with permission from ref 151. Copyright 2020 Elsevier B.V.

where θ_d is the deviation angle of the fracturing fracture, and P_w is the injection pressure.

High injection pressure can facilitate the tearing and expansion of rock formations, but it may also lead to environmental concerns. To maximize the effectiveness of fracturing fracture propagation, it is necessary to consider temperature factors and select appropriate parameters based on actual conditions. Close monitoring of temperature changes, as well as the response of fluids and rocks, is also essential.[152]

3.3. Injection Rate and Displacement. During the fluid injection process, there is a strong interaction between the fracturing fracture and pre-existing discontinuities, resulting in complex geometric shapes of the fracture. At low injection rates, the fluid pressure may not be high enough to open bedding planes. The injection rate can influence the direction of fracture propagation. With increasing injection rate, it is easier to generate branching fractures and activate natural fractures, leading to the formation of geometrically complex fractures. Additionally, when the injection rate is sufficiently high, the fracture expansion path tends to follow the direction of maximum horizontal stress, which helps overcome the influence of natural fractures to some extent.[34,153] At low injection rates, hydraulic fracturing primarily generates longitudinal and multitransverse fractures. Fracture density is often used to quantify geometric complexity. When the injection rate varies in the range of 0.01−1.0 m^3/min, the fracture density in the horizontal section is generally lower than the fracture density in the vertical section.[123,133] The injection rate of fracturing fluid also affects the curvature of the fractures. The higher is the injection rate, the smaller is the curvature of the fracturing fractures. Under the same injection volume, higher injection rates lead to wider fractures and shorter lengths (Figure 26). Meanwhile, without considering the injection volume, higher injection rates result in a broader expansion of the fractures.[92,110]

During the fracturing process, as the injection volume increases, the average width of the fractures gradually increases, while the average height of the fractures initially increases and

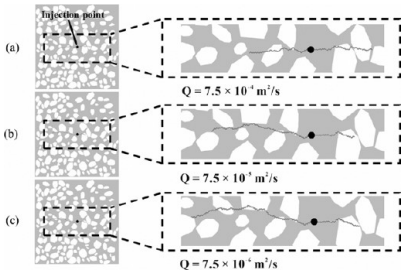

Figure 26. Hydraulic fracture morphology of glutenite under different injection rates: (a) $Q = 7.5 \times 10^{-4}$ m^2/s, (b) $Q = 7.5 \times 10^{-5}$ m^2/s, and (c) 7.5×10^{-6} m^2/s. Reprinted with permission from ref 92. Copyright 2023 Elsevier B.V.

https://doi.org/10.1021/acsomega.3c08547
ACS Omega 2024, 9, 117−136

then levels off. Typically, larger injection volumes lead to the formation of larger and longer fractures, and expand the fractures onto a greater rock surface area. This can increase the number and length of flow paths, enhancing fracture activity over a longer period of time. However, larger injection volumes can also result in uneven distribution of the fluid within the fractures, affecting the overall shape and stability of the fractures.[154]

4. FRACTURE PROPAGATION MODEL AND SIMULATION

4.1. Fracture Propagation Model. Hydraulic fracturing is characterized by three two-dimensional theoretical models, including the PK model,[155] PKN model,[156] and KGD model.[157,158] However, due to the oversimplified assumptions of these three models, they cannot meet the requirements of industrial development. The P3D model has emerged to simultaneously simulate the expansion of fracture in both lateral and longitudinal directions[159,160] (Figure 27). In recent

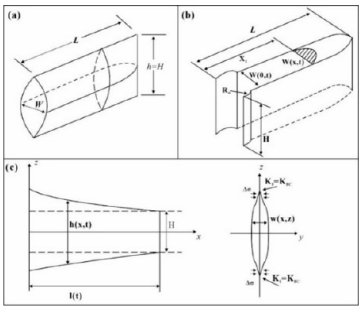

Figure 27. Basic schematic diagrams of hydraulic fracture propagation models: (a) PKN model, (b) KGD model, and (c) P3D model. Reprinted with permission from ref 159. Copyright 2023 Editorial Department of China Coal Society Journal.

years, with the advancement of computers, unconventional fracture models, OpenT models, and others have emerged, greatly expanding the organic integration of theory and field monitoring data. (1) In the PKN model, fractures have a fixed height and an elliptical cross-section, and they propagate only in the longitudinal direction. Its expression is as follows:

$$\frac{Q_0 t}{2h} = \int_0^{l(t)} w\,\mathrm{d}x + 2C' \int_0^{l(t)} \sqrt{t - t_0(x)}\,\mathrm{d}x \tag{3}$$

where Q_0 is the inlet injection rate; l is the fracture length; C' is $2C_L$; C_L is the leak-off coefficient; $t_0(x)$ is the time fluid passes through point x; w is the fracture width; and x is the horizontal coordinate.

(2) The KGD model requires the following assumptions: (a) constant fracture height; (b) rectangular fracture cross-section with elliptical lateral sides; (c) sharp front tip of the fracture; and (d) consideration of rock stiffness only in the horizontal plane. The expression for the KGD model is as follows:

$$L = 0.8413\left(\frac{8GQ^3}{(1-\nu)\mu}\right)^{1/6} t^{2/3}$$

$$W_0 = 0.44\left(\frac{8(1-\nu)Q^3\mu}{G}\right)^{1/6} t^{1/3}$$

$$P_w = \sigma_{\min} + 0.242\left(\frac{2G^3Q\mu}{(1-\nu)^3L^2}\right)^{1/4} \tag{4}$$

where G is the shear modulus, MPa; ν is Poisson's ratio; μ is the fluid viscosity, mPa s; $\sigma_{\min}$ is the minimum horizontal principal stress, MPa; Q is the pumping rate, m^3/min; t is the construction time, min; L is the fracture length, m; W_0 is the fracture width, m; and P_w is the bottomhole pressure, MPa.

(3) The P3D model evolves from the PKN model and no longer assumes a fixed fracture height. It reduces the complete 3D elastic rock response to a 2D deformation problem by setting the elastic plane strain on each vertical cross-section.[160] However, it does not consider the changes in the geometric shape of the fractures in 3D space; hence, it is referred to as a pseudo-three-dimensional model. (4) The unconventional fracture model considers the stress interference effect between adjacent hydraulic fractures and simulates the comprehensive behavior of fracture propagation, rock deformation, and fluid flow in the complex fracture network generated during hydraulic fracturing. The UFM model assumes that the reservoir has uniform elastic properties and averages the values over all layers containing fracture height.[161] (5) The OpenT model is a new fracture interaction analysis model that considers both the fracture toughness of the rock and the permeability of natural fractures.[162] This model focuses on quantitatively describing the geometric changes and geo-mechanical characteristics of natural fractures caused by hydraulic fracture contact. The OpenT model is highly sensitive to parameters such as injection fluid and fracture length. Additionally, due to minimal fluid loss in natural fractures, high injection rates or fluid viscosities greatly increase the likelihood of penetrating natural fractures.

As shown in Table 6, there are significant differences and shortcomings among different calculation models. Traditional hydraulic fracturing calculation models such as PKN, KGD, and P3D are based on the study of single fracture propagation and cannot handle the problem of multiple fractures. Although the UFM and OpenT models can compute the expansion behavior of complex fracture networks in three-dimensional space, their expansion paths are limited and their accuracy needs to be improved (Table 6).

4.2. Fracture Propagation Simulation. Research on hydraulic fracture propagation is typically done through physical and numerical simulations. Physical simulations often involve the use of true triaxial fracturing apparatus combined with techniques such as acoustic emission or CT scanning.[124,163] However, physical simulations face challenges such as sampling difficulties, laboratory constraints, and scale effects.[92,164] Additionally, physical simulations can only reveal the phenomenon of fracture propagation without quantitatively uncovering the laws governing fracture propagation.

Most studies rely on numerical simulations, which play a crucial role in investigating fracture propagation (Table 7). There are two main approaches in numerical simulations. One approach considers the discontinuous nature of rocks,

https://doi.org/10.1021/acsomega.3c08547
ACS Omega 2024, 9, 117−136

Table 6. Characteristics and Applicability of the Classical Theory Calculation Model for Hydraulic Fracturing[159]

model	characteristics	applicability	shortcoming
PKN model	assuming fracture toughness does not affect the geometric shape of the fracture, and since there is no fluid flow in the vertical plane, the pressure is uniform	applicable when the fracture height is higher than the fracture length	the effects of fracture mechanics and fracture tip effect are not considered
KGD model	assume that the fracture width is uniform in the vertical direction	applicable to fractures where the horizontal penetration force is lower than the vertical penetration force, and the aspect ratio is less than 1	the vertical fracture expansion is limited by the changes in material properties and the minimum horizontal in situ stress
P3D model	this model removes the assumption of a fixed fracture height and explains the height variation by considering field stress contrast, rock toughness, and local net fluid pressure	applicable to simulate the simultaneous expansion process of fracture height and length direction	the orientation of the fracture is fixed, and no consideration is given to the variation of the fracture's geometric shape in three-dimensional space
UFM model	the reservoir is assumed to have uniform elastic properties, and the stress interference effect between adjacent hydraulic fractures is considered	applicable for simulating the combined behavior of rock deformation and fluid flow	the effect of permeability and pore pressure on fluid loss in natural fractures is not considered
OpenT model	simultaneously considering the fracture toughness of the rock and the permeability of natural fractures	applicable for calculating the initiation and propagation of hydraulic fractures through natural fractures during the hydraulic fracturing process	the effect of solid elastic deformation is not considered

employing methods such as FEDM, XFEM, and DEM. The other approach treats the reservoir rock as a continuous medium, using methods like the FEM, BEM, and FDM.[96] Different methods have different applicability conditions. For instance, DEM, which considers particle-scale effects, may not be suitable for reservoir-scale computations. However, XFEM, which utilizes function-based approaches, exhibits clear advantages in fracturing simulations.[165] FDEM, which combines finite element solutions for deformation problems with DEM for simulating interblock contact, has been increasingly applied in fracture propagation studies in recent years (Figure 28).[166−169]

5. CONCLUSION AND EXPECTATION

5.1. Conclusion. (1) The expansion of fracturing fractures is a comprehensive process constrained by factors such as lithology and mineral composition, water saturation, heterogeneity, natural weak planes, and in situ stresses. Specifically, (a) different lithologies exhibit different characteristics of fracture expansion and fracture network. (b) Interactions between natural fractures and fracturing fractures may involve behaviors such as crossing, propagation, and capturing, and are influenced by geological factors such as approach angle, principal stress difference, rock strength, and self-cementation, as well as engineering factors such as injection rate, type of fracturing fluid, and temperature. (c) The thickness of the formation and the in situ stress state also affect the law of fracture expansion, and a high confining pressure can make it difficult for fractures to initiate.

(2) Various geological factors collectively influence the laws and characteristics of fracturing, such as the length of fractures, the direction of fracture propagation, and the complexity of fracture networks. However, there is a lack of a standardized quantitative evaluation for the impact of these factors on fracture propagation, and there is insufficient research on lithologies other than shale in fracturing.

(3) The type of fracturing fluid, injection rate, injection volume, and temperature have significant control over fracture propagation. As compared to water-based fracturing fluids, CO_2 generates more complex fracture. Additionally, the type of fracturing fluid and temperature can alter the mechanical properties of different rock, thereby affecting the laws of fracture propagation.

(4) The existing models for fracture expansion have certain limitations. Traditional models such as PKN, KGD, and P3D are essentially 2-D models and cannot be widely applied in production. Moreover, these models are typically used for single fracture expansion and have difficulty in handling complex fracture networks. Moreover, unconventional fracture models and OpenT models have organically combined theoretical models with microseismic monitoring data, allowing for the consideration of multiple geological factors on hydraulic fracture networks. However, these models still rely on idealized assumptions regarding fracture morphology and propagation paths, and their computational reliability needs further validation.

(5) Numerical simulation has the potential to surpass the limitations of physical simulation and characterize the expansion of fractures under the influence of multiple paths, geological factors, engineering factors, and in situ reservoir conditions. However, different simulation methods have different drawbacks and applicability.

https://doi.org/10.1021/acsomega.3c08547
ACS Omega 2024, 9, 117−136

Table 7. Comprehensive Comparison of Numerical Simulation Methods for Fracture Propagation[170,a]

	continuous medium methods								discrete medium methods	
	FEM-based					BEM-based	FDM-based	FDEM-based		
comparison items	ARM	XFEM	CZM	PFM	DEL	DDM	FDM	FDEM	PFC	UDEC
rock heterogeneity	Y	Y	Y	Y	Y	N	Y	Y	Y	Y
weak planes	Y	Y	Y	Y	Y	Y	Y	Y	Y	Y
fracture initiation	Y	N	Y	Y	Y	N	Y	Y	Y	Y
multi fracture propagation	√√√	√	√√	√	√	√	√	√√	√√	√√
multifield coupling	√	√	√	√	√	√√√	√	√√	√√√	√√√
fracture parameter acquisition	√√√	√	√√	√√	√√√	√	√	√√	√√√	√√√
computational workload	√√√	√√	√√	√√	√√	√	√	√√	√√√	√√√
suitable scale	lab-scale	lab-scale	lab-scale	lab-scale	lab-scale	field-scale	field-scale	micro-Scale	micro-Scale	micro-Scale
auxiliary software/code	N	ABAQUS	ABAQUS	COMSOL	COMSOL	Resfrac	FLAC3D	MultiFracS	PFC2D/PFC3D	UDEC

[a]Note: Y, yes; N, no; √, easy/low; √√, general; √√√, difficult/high.

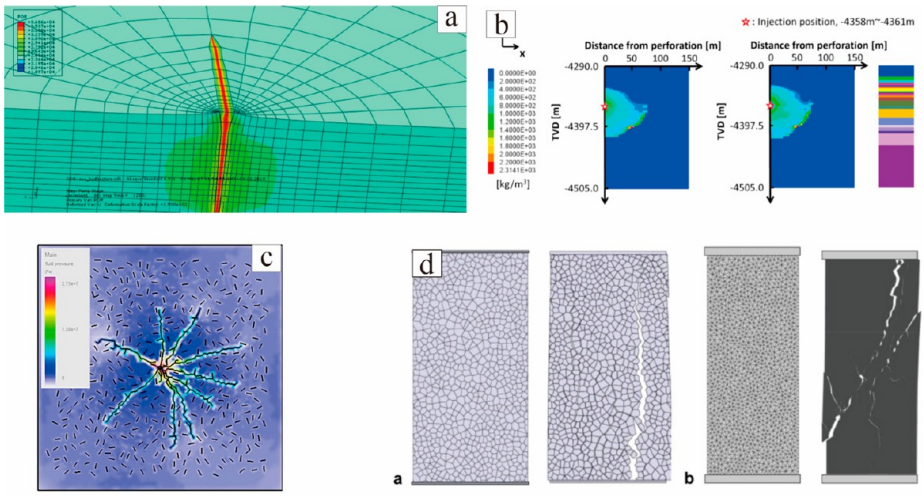

Figure 28. Results of different numerical simulation methods: (a) ABAQUS, (b) FLAC 3D, (c) MultiFracS, and (d) UDEC.[171−173]

5.2. Expectation. (1) Research on heterogeneity is mostly conducted in three-dimensional space, introducing convolutional identification of minerals or AM technology to identify minerals and establish three-dimensional models. The search for quantitative parameters to characterize heterogeneity in three-dimensional space, combined with simulation software, is an important direction for studying the impact of heterogeneity on fracture propagation.

(2) During fracturing operations, the development of fractures has a substantial impact on its compressibility. The establishment of a multiscale fracture network model for natural fracture systems is currently a challenging research problem. Therefore, it is worth considering the use of computer technology to establish quantitative models based on the characteristics of natural fractures.

(3) The phase transition of CO_2 can cause the expansion of SC-CO_2 and induce more complex fractures. At the same time, SC-CO_2 is extremely sensitive to temperature and pressure. Analyzing the expansion of induced fractures during SC-CO_2 fracturing requires considering the phase transition during the process. It is of great significance to establish a THL coupled equation for numerical simulation of fractures.

(4) While the current hydraulic fracturing theoretical calculation models have achieved rich research results in the influence of geological parameters and the interaction of multiple fractures, how the interaction mode of fractures combines with the geometric morphology of natural fractures, and how it is affected by fracturing engineering parameters such as injection rate and fracturing fluid viscosity in three-dimensional space, remain key areas of future research.

(5) Geological-engineering integration is an important principle in fracturing design, implementation, and postevaluation. However, as fracture propagation continues, the reservoir parameters of fracture communication will inevitably undergo certain changes. Therefore, it is necessary to further upgrade the previous geological-engineering integration to dynamic geological-engineering integration. This is a major direction for future research, aiming to achieve real-time and dynamic description of the fracture morphology, geometric dimensions, and reservoir geological parameters throughout the entire hydraulic fracturing process. This will enable the adjustment of fracturing parameters to achieve timely and dynamic optimal matching between fracture parameters and reservoir parameters, thereby maximizing the exploitation potential of the reservoir.

https://doi.org/10.1021/acsomega.3c08547
ACS Omega 2024, 9, 117−136

AUTHOR INFORMATION

Corresponding Authors

Changcheng Han − *College of Geology and Mining Engineering, Xinjiang University, Urumqi 830047, China*; Email: hanchangchen@126.com

Bo Wei − *No.156 Geological Exploration Team, Xinjiang Uygur Autonomous Region Coalfield Geology Bureau, Urumqi 830047, China*; Email: weibo156@126.com

Authors

Geng Liu − *College of Geology and Mining Engineering, Xinjiang University, Urumqi 830047, China*; orcid.org/0009-0005-1572-1729

Huijie Yang − *Research Institute of Exploration and Development, Qinghai Oilfield, Jiuquan 735000, China*

Jinlei Xiu − *Exploration and Development Research, Institute of Shengli Oilfield, Dongying, Shandong 257022, China*

Xin Li − *College of Geology and Mining Engineering, Xinjiang University, Urumqi 830047, China*

Zhiwei Hao − *Exploration and Development Research, Institute of Shengli Oilfield, Dongying, Shandong 257022, China*

Ning Lv − *National 305 Project Office, Science and Technology Department of Xinjiang Uygur Autonomous Region, Urumqi 830047, China*

Complete contact information is available at: https://pubs.acs.org/10.1021/acsomega.3c08547

Notes

The authors declare no competing financial interest.

ACKNOWLEDGMENTS

We would like to extend our gratitude to the Autonomous region graduate student innovation project (grant no. XJ2023G112). Our thanks also go to the anonymous reviewers for their insightful and constructive comments for improving the manuscript.

REFERENCES

(1) Cui, X.; Bustin, A. M. M.; Bustin, R. M. Measurements of gas permeability and diffusivity of tight reservoir rocks: different approaches and their applications. *Geofluids* **2009**, *9* (3), 208−223.

(2) Gale, J. F. W.; Laubach, S. E.; Olson, J. E.; Eichhuble, P.; Fall, A. Natural Fractures in shale: A review and new observations. *AAPG Bulletin* **2014**, *98* (11), 2165−2216.

(3) Mojid, M. R.; Negash, B. M.; Abdulelah, H.; Jufar, S. R.; Adewumi, B. K. A state - of - art review on waterless gas shale fracturing technologies. *J. Pet. Sci. Eng.* **2021**, *196*, 108048.

(4) Barati, R.; Liang, J.-T. A review of fracturing fluid systems used for hydraulic fracturing of oil and gas wells. *J. Appl. Polym. Sci.* **2014**, *131* (16), 40735.

(5) Sleytr, U.; Robards, A. Freeze-fracturing: A review of methods and results. *J. Microsc.* **1977**, *111*, 77−100.

(6) Cheng, S.; Zhang, M.; Zhang, X.; Wu, B.; Chen, Z.; Lei, Z.; Tan, P. Numerical study of hydraulic fracturing near a wellbore using dual boundary element method. *International Journal of Solids and Structures* **2022**, *239−240*, 111479.

(7) Deng, B.; Yin, G.; Zhang, D.; Li, M.; Liu, Y.; Lu, J. Experimental investigation of fracture propagation induced by carbon dioxide and water in coal seam reservoirs. *Powder Technol.* **2018**, *338*, 847−856.

(8) Yi, L.-P.; Waisman, H.; Yang, Z.-Z.; Li, X.-G. A consistent phase field model for hydraulic fracture propagation in poroelastic media. *Computer Methods in Applied Mechanics and Engineering* **2020**, *372*, 113396.

(9) Dang, Y.; Wu, Y.; Wang, T.; Cui, X.; An, D. Energy and damage evolution characteristics of rock materials under different water content. *Chin. J. High Pressure Phys.* **2023**, *37*, 62−71.

(10) Li, D.; Wang, W. Quantitative analysis of the influence of saturation on rock strength reduction considering the distribution of water. *Geomechanics and Geophysics for Geo-Energy and Geo-Resources* **2019**, *5* (2), 197−207.

(11) Dehghan, A. N.; Goshtasbi, K.; Ahangari, K.; Jin, Y. Mechanism of fracture initiation and propagation using a tri-axial hydraulic fracturing test system in naturally fractured reservoirs. *European Journal of Environmental and Civil Engineering* **2016**, *20* (5), 560−585.

(12) Dehghan, A. N.; Goshtasbi, K.; Ahangari, K.; Jin, Y.; Bahmani, A. 3D Numerical Modeling of the Propagation of Hydraulic Fracture at Its Intersection with Natural (Pre-existing) Fracture. *Rock Mechanics and Rock Engineering* **2017**, *50* (2), 367−386.

(13) Ju, Y.; Wang, Y.; Xu, B.; Chen, J.; Yang, Y. Numerical analysis of the effects of bedded interfaces on hydraulic fracture propagation in tight multilayered reservoirs considering hydro-mechanical coupling. *J. Pet. Sci. Eng.* **2019**, *178*, 356−375.

(14) Wang, C.; Wang, J. G. Effect of heterogeneity and injection borehole location on hydraulic fracture initiation and propagation in shale gas reservoirs. *Journal of Natural Gas Science and Engineering* **2021**, *96*, 104311.

(15) Kahrilas, G. A.; Blotevogel, J.; Stewart, P. S.; Borch, T. Biocides in Hydraulic Fracturing Fluids: A Critical Review of Their Usage, Mobility, Degradation, and Toxicity. *Environ. Sci. Technol.* **2015**, *49* (1), 16−32.

(16) Vengosh, A.; Jackson, R. B.; Warner, N.; Darrah, T. H.; Kondash, A. A Critical Review of the Risks to Water Resources from Unconventional Shale Gas Development and Hydraulic Fracturing in the United States. *Environ. Sci. Technol.* **2014**, *48* (15), 8334−8348.

(17) Luca, G. An Overview of Hydraulic Fracturing and Other Formation Stimulation Technologies for Shale Gas Production, 2013.

(18) Lester, Y.; Ferrer, I.; Thurman, E. M.; Sitterley, K. A.; Korak, J. A.; Aiken, G.; Linden, K. G. Characterization of hydraulic fracturing flowback water in Colorado: Implications for water treatment. *Science of The Total Environment* **2015**, *512−513*, 637−644.

(19) Fu, C.; Liu, N. Waterless fluids in hydraulic fracturing - A review. *Journal of Natural Gas Science and Engineering* **2019**, *67*, 214−224.

(20) Li, C.; Huang, Y.; Sun, X.; Gao, R.; Zeng, F.; Tontiwachwuthikul, P.; Liang, Z. Rheological properties study of foam fracturing fluid using CO2 and surfactant. *Chem. Eng. Sci.* **2017**, *170*, 720−730.

(21) Monjezi, K.; Mohammadi, M.; Khaz'ali, A. R. Stabilizing CO2 foams using APTES surface-modified nanosilica: Foamability, foaminess, foam stability, and transport in oil-wet fractured porous media. *J. Mol. Liq.* **2020**, *311*, 113043.

(22) Zhang, Z.; Mao, J.; Yang, X.; Zhao, J.; Smith, G. S. Advances in waterless fracturing technologies for unconventional reservoirs. *Energy Sources, Part A: Recovery, Utilization, and Environmental Effects* **2019**, *41*, 237−251.

(23) Hou, B.; Diao, C.; Li, D. An experimental investigation of geomechanical properties of deep tight gas reservoirs. *Journal of Natural Gas Science and Engineering* **2017**, *47*, 22−33.

(24) Song, M.; Shao, T.; Li, J.; Ji, S.; Wang, Q. Experimental study of deformation of Carrara marble at high pressure and high temperature. *Acta Petrologica Sinica* **2014**, *30*, 589−596.

(25) Bakhshi, E.; Rasouli, V.; Ghorbani, A.; Fatehi Marji, M.; Damjanac, B.; Wan, X. Lattice Numerical Simulations of Lab-Scale Hydraulic Fracture and Natural Interface Interaction. *Rock Mechanics and Rock Engineering* **2019**, *52* (5), 1315−1337.

(26) Zou, J.; Jiao, Y.-Y.; Tang, Z.; Ji, Y.; Yan, C.; Wang, J. Effect of mechanical heterogeneity on hydraulic fracture propagation in unconventional gas reservoirs. *Computers and Geotechnics* **2020**, *125*, 103652.

(27) Zhang, X.; Wu, B.; Jeffrey, R. G.; Connell, L. D.; Zhang, G. A pseudo-3D model for hydraulic fracture growth in a layered rock.

International Journal of Solids and Structures **2017**, *115*−*116*, 208−223.
(28) Zhou, S.; Zhuang, X.; Rabczuk, T. Phase-field modeling of fluid-driven dynamic cracking in porous media. *Computer Methods in Applied Mechanics and Engineering* **2019**, *350*, 169−198.
(29) Huang, L.; Dontsov, E.; Fu, H.; Lei, Y.; Weng, D.; Zhang, F. Hydraulic fracture height growth in layered rocks: Perspective from DEM simulation of different propagation regimes. *International Journal of Solids and Structures* **2022**, *238*, 111395.
(30) Qin, M.; Yang, D.; Chen, W.; Yang, S. Hydraulic fracturing model of a layered rock mass based on peridynamics. *Engineering Fracture Mechanics* **2021**, *258*, 108088.
(31) Zhou, D.; Zhang, G. A review of mechanisms of induced fractures in SC-CO fracturing. *Petroleum Sci. Bull.* **2020**, *5*, 239−253.
(32) Gao, J.; Hou, B.; Chen, M.; Fu, W.; Wu, Y.; Zhang, R. Effects of rock strength and interfacial property on fracture initiation and propagation. *Chin. J. Rock Mechanics Eng.* **2018**, *37*, 4108−4114.
(33) Zeng, L.; Ma, S.; Tian, H.; Xue, M.; Liu, G.; Lu, W. Research Progress of Natural Fractures in Organic Rich Shale. *Earth Sci.* **2023**, *48*, 2427−2442.
(34) Xiong, D.; Ma, X. Influence of natural fractures on hydraulic fracture propagation behaviour. *Engineering Fracture Mechanics* **2022**, *276*, 108932.
(35) Zhao, K.; Ran, S.; Zeng, P.; Yang, D.; Teng, T. Effect of moisture content on characteristic stress and acoustic emission characteristics of red sandstone. *Rock Soil Mechanics* **2021**, *42*, 889−908.
(36) Chen, S.; Liu, Y.; Zhang, J.; Li, P.; Tang, X.; Li, Z.; Dong, Z.; Xu, L.; Zhao, X. Formation conditions and evolution of fractures in multiple tight rocks: Implications for unconventional reservoir exploitation. *J. Pet. Sci. Eng.* **2021**, *200*, 108354.
(37) Hou, Z.-K.; Cheng, H.-L.; Sun, S.-W.; Chen, J.; Qi, D.-Q.; Liu, Z.-B. Crack propagation and hydraulic fracturing in different lithologies. *Applied Geophysics* **2019**, *16* (2), 243−251.
(38) Breyer, J. A.; Alsleben, H.; Enderlin, M. B. Predicting Fracability in Shale Reservoirs, 2011.
(39) Mullen, M.; Enderlin, M. Fracability Index - More Than Just Calculating Rock Properties. *SPE Annual Technical Conference and Exhibition*, 2012; p SPE-159755-MS.
(40) Zeng, Z.; Liu, Z.; Ma, J.; Zhang, C.; Li, J.; Liu, Z.; Sun, L. A New Method for Fracrability Evaluation in Deep and Tight Sandstone Reservoirs. *J. Geomechanics* **2019**, *25*, 223−232.
(41) Zhao, J.; Xu, W.; Li, Y.; Hu, J.; Li, J. A New Method for Fracability Evaluation of Shale-gas Reservoirs. *Natural Gas Geoscience* **2015**, *26*, 1165−1172.
(42) Feng, X.; Zhao, W.; Wang, T. Micromechanical Analysis and Brittleness Evaluation of Heterogeneous tight Reservoir. *Special Oil Gas Reservoirs* **2019**, *26*, 113−117.
(43) Meng, F.; Zhou, H.; Zhang, C.; Xu, R.; Lu, J. Evaluation Methodology of Brittleness of Rock Based on Post-Peak Stress-Strain Curves. *Rock Mechanics and Rock Engineering* **2015**, *48* (5), 1787−1805.
(44) Jarvie, D. M.; Hill, R. J.; Ruble, T. E.; Pollastro, R. M. Unconventional shale-gas systems: The Mississippian Barnett Shale of north-central Texas as one model for thermogenic shale-gas assessment. *AAPG Bulletin* **2007**, *91* (4), 475−499.
(45) Wen, M.; Huang, H.; Hou, Z.; Wang, F.; Qiu, H.; Ma, N.; Zhou, S. Numerical simulation of the non-Newtonian fracturing fluid influences on the fracture propagation. *Energy Science & Engineering* **2022**, *10* (2), 404−413.
(46) Xu, X.; Kim, J. J.; Li, Y.; Xie, J.; Shao, C.; Wei, J.-J. Oxidative stress-induced miRNAs modulate AKT signaling and promote cellular senescence in uterine leiomyoma. *Journal of Molecular Medicine* **2018**, *96* (10), 1095−1106.
(47) Wu, M. Y.; Zhang, D. M.; Wang, W. S.; Li, M. H.; Liu, S. M.; Lu, J.; Gao, H. Numerical simulation of hydraulic fracturing based on two-dimensional surface fracture morphology reconstruction and combined finite-discrete element method. *Journal of Natural Gas Science and Engineering* **2020**, *82*, 103479.
(48) Zhao, H.; Li, W.; Wang, L.; Fu, J.; Xue, Y. L.; Zhu, J. J.; Li, S. Q. The Influence of the Distribution Characteristics of Complex Natural Fracture on the Hydraulic Fracture Propagation Morphology. *Frontiers in Earth Science* **2022**, *9*, 1 DOI: 10.3389/feart.2021.784931.
(49) Mavko, G.; Mukerji, T.; Dvorkin, J. *Rock Physics Handbook: Tools for Seismic Analysis of Porous Media*; Cambridge University Press: Cambridge, 2003.
(50) Guha Roy, D.; Singh, T. N.; Kodikara, J. Influence of joint anisotropy on the fracturing behavior of a sedimentary rock. *Engineering Geology* **2017**, *228*, 224−237.
(51) Jin, X.; Shah, S. N.; Roegiers, J.-C.; Zhang, B. *Fracability Evaluation in Shale Reservoirs - An Integrated Petrophysics and Geomechanics Approach*; SPE Hydraulic Fracturing Technology Conference, 2014.
(52) Mahanta, B.; Tripathy, A.; Vishal, V.; Singh, T. N.; Ranjith, P. G. Effects of strain rate on fracture toughness and energy release rate of gas shales. *Engineering Geology* **2017**, *218*, 39−49.
(53) Zhao, X.; Huang, B.; Xu, J. Experimental investigation on the characteristics of fractures initiation and propagation for gas fracturing by using air as fracturing fluid under true triaxial stresses. *Fuel* **2019**, *236*, 1496−1504.
(54) Zhang, D.; Ranjith, P. G.; Perera, M. S. A. The brittleness indices used in rock mechanics and their application in shale hydraulic fracturing: A review. *J. Pet. Sci. Eng.* **2016**, *143*, 158−170.
(55) Zhao, X.; Zeng, L.; Zu, K.; Hu, X.; Jiao, J.; Zhu, L.; Shi, J. Brittleness characteristics and its control on natural fractures in tight reservoirs: A case study from Chang 7 tight reservoir in Longdong area of the Ordos Basin. *Oil Gas Geol.* **2016**, *37*, 62−71.
(56) Andreev, G. E. *Brittle Failure of Rock Materials*; CRC Press: New York, 1995.
(57) Honda, H.; Sanada, Y. Hardness of coal. *Fuel* **1956**, *35*, 451−461.
(58) Protodyakonov, M. *Mechanical Properties and Drillability of Rocks*; Proceedings of the 5th Symposium on Rock Mechanics, University of Minnesota Minneapolis: MN, 1962; p 118.
(59) Quinn, J. B.; Quinn, G. D. Indentation brittleness of ceramics: a fresh approach. *J. Mater. Sci.* **1997**, *32* (16), 4331−4346.
(60) Hucka, V.; Das, B. Brittleness determination of rocks by different methods. *International Journal of Rock Mechanics and Mining Sciences & Geomechanics Abstracts* **1974**, *11* (10), 389−392.
(61) Bishop, A. *Progressive Failure-with Special Reference to the Mechanism Causing It*; Proc. Geotech. Conf.: Oslo, 1967; pp 142−150.
(62) Jin, X.; Shah, S.; Truax, J.; Roegiers, J.-C. *A Practical Petrophysical Approach for Brittleness Prediction from Porosity and Sonic Logging in Shale Reservoirs*; SPE Annual Technical Conference and Exhibition, 2014.
(63) Yang, B.; Wang, H.; Shen, Z.; Olorode, O.; Wang, B.; Zheng, Y.; Yan, W.; Jia, Z. Full-Sample X-ray Microcomputed Tomography Analysis of Supercritical CO2 Fracturing in Tight Sandstone: Effect of Stress on Fracture Dynamics. *Energy Fuels* **2021**, *35* (2), 1308−1321.
(64) Rickman, R.; Mullen, M.; Petre, J.; Grieser, W.; Kundert, D. A Practical Use of Shale Petrophysics for Stimulation Design Optimization: All Shale Plays Are Not Clones of the Barnett Shale, 2008.
(65) Luan, X.; Di, B.; Wei, J.; Li, X.; Qian, K.; Xie, J.; Ding, P. Laboratory measurements of brittleness anisotropy in synthetic shale with different cementation. *SEG Technical Program Expanded Abstracts* **2014**, 3005−3009.
(66) Sun, S. Z.; Wang, K. N.; Yang, P.; Li, X. G.; Sun, J. X.; Liu, B. H.; Jin, K. *Integrated Prediction of Shale Oil Reservoir Using Pre-Stack Algorithms for Brittleness and Fracture Detection*; International Petroleum Technology Conference, 2013.
(67) Tarasov, B.; Potvin, Y. Universal criteria for rock brittleness estimation under triaxial compression. *International Journal of Rock Mechanics and Mining Sciences* **2013**, *59*, 57−69.
(68) Guo, Z.; Li, X.; Chapman, M. Exploring the Effect of Fractures and Microstructure on Brittleness Index in the Barnett Shale. *2012 SEG Annual Meeting* 2012; p SEG-2012−0771.

https://doi.org/10.1021/acsomega.3c08547
ACS Omega 2024, 9, 117−136

(69) Chen, J.; Zhang, G.; Chen, H.; Yin, X. *The Construction of Shale Rock Physics Effective Model and Prediction of Rock Brittleness*; 2014 SEG Annual Meeting, 2014.
(70) Wang, F. P.; Gale, J. F. W. Screening Criteria for Shale-Gas Systems, 2009.
(71) Bieniawski, Z. T. Mechanism of brittle fracture of rock: Part I—theory of the fracture process. *International Journal of Rock Mechanics and Mining Sciences & Geomechanics Abstracts* **1967**, *4* (4), 395−406.
(72) Bieniawski, Z. T. Mechanism of brittle fracture of rock: Part II—experimental studies. *International Journal of Rock Mechanics and Mining Sciences & Geomechanics Abstracts* **1967**, *4* (4), 407−423.
(73) Cai, M.; Kaiser, P. K.; Tasaka, Y.; Maejima, T.; Morioka, H.; Minami, M. Generalized crack initiation and crack damage stress thresholds of brittle rock masses near underground excavations. *International Journal of Rock Mechanics and Mining Sciences* **2004**, *41* (5), 833−847.
(74) Moradian, Z.; Einstein, H. H.; Ballivy, G. Detection of Cracking Levels in Brittle Rocks by Parametric Analysis of the Acoustic Emission Signals. *Rock Mechanics and Rock Engineering* **2016**, *49* (3), 785−800.
(75) Zhang, D.; Pathegama Gamage, R.; Perera, M. S. A.; Zhang, C.; Wanniarachchi, W. A. M. Influence of Water Saturation on the Mechanical Behaviour of Low-Permeability Reservoir Rocks. *Energies* **2017**, *10* (2), 236.
(76) Duda, M.; Renner, J. The weakening effect of water on the brittle failure strength of sandstone. *Geophysical Journal International* **2013**, *192* (3), 1091−1108.
(77) Zhang, X.; Lu, Y.; Tang, J.; Zhou, Z.; Liao, Y. Experimental study on fracture initiation and propagation in shale using supercritical carbon dioxide fracturing. *Fuel* **2017**, *190*, 370−378.
(78) Wong, L. N. Y.; Maruvanchery, V.; Liu, G. Water effects on rock strength and stiffness degradation. *Acta Geotechnica* **2016**, *11* (4), 713−737.
(79) Zhuang, L.; Kim, K. Y.; Diaz, M.; Yeom, S. Evaluation of water saturation effect on mechanical properties and hydraulic fracturing behavior of granite. *International Journal of Rock Mechanics and Mining Sciences* **2020**, *130*, 104321.
(80) Gale, J. F. W.; Reed, R. M.; Holder, J. Natural fractures in the Barnett Shale and their importance for hydraulic fracture treatments. *AAPG Bulletin* **2007**, *91* (4), 603−622.
(81) Ross, D. J. K.; Marc Bustin, R. The importance of shale composition and pore structure upon gas storage potential of shale gas reservoirs. *Marine and Petroleum Geology* **2009**, *26* (6), 916−927.
(82) Chugh, Y. P.; Missavage, R. A. Effects of moisture on strata control in coal mines. *Engineering Geology* **1981**, *17* (4), 241−255.
(83) Erguler, Z. A.; Ulusay, R. Water-induced variations in mechanical properties of clay-bearing rocks. *International Journal of Rock Mechanics and Mining Sciences* **2009**, *46* (2), 355−370.
(84) Hadizadeh, J.; Law, R. D. Water-weakening of sandstone and quartzite deformed at various stress and strain rates. *International Journal of Rock Mechanics and Mining Sciences & Geomechanics Abstracts* **1991**, *28* (5), 431−439.
(85) Josh, M.; Esteban, L.; Delle Piane, C.; Sarout, J.; Dewhurst, D. N.; Clennell, M. B. Laboratory characterisation of shale properties. *J. Pet. Sci. Eng.* **2012**, *88*−*89*, 107−124.
(86) Yao, Q.; Chen, T.; Ju, M.; Liang, S.; Liu, Y.; Li, X. Effects of Water Intrusion on Mechanical Properties of and Crack Propagation in Coal. *Rock Mechanics and Rock Engineering* **2016**, *49* (12), 4699−4709.
(87) Pan, Z.; Connell, L. D.; Camilleri, M.; Connelly, L. Effects of matrix moisture on gas diffusion and flow in coal. *Fuel* **2010**, *89* (11), 3207−3217.
(88) Zhang, C.; Zhao, Q.; Wang, L.; Zhao, N.; YU, Y. Test and numerical modeling on strain softening behavior and permeability evolution of rock under tri-axial compression. *J. China Coal Soc.* **2015**, *40*, 1774−1782.
(89) Fossen, H. *Structural Geology*, 2nd ed.; Cambridge University Press: Cambridge, 2016.
(90) Sharafisafa, M.; Sato, A.; Aliabadian, Z. Hydraulic fracture development in conglomerate reservoirs simulated using combined finite-discrete element method. *Engineering Fracture Mechanics* **2023**, *279*, 109063.
(91) Yu, M.; Zhu, W.; YU, Y.; Yu, Q. Numerical Simulation for Calculating the Tensile Strength and Fracture Toughness Based on Different Grain Sizes. *Journal of Northeastern University (Natural Science)* **2017**, *38*, 864−868.
(92) Huang, L.; He, R.; Yang, Z.; Tan, P.; Chen, W.; Li, X.; Cao, A. Exploring hydraulic fracture behavior in glutenite formation with strong heterogeneity and variable lithology based on DEM simulation. *Engineering Fracture Mechanics* **2023**, *278*, 109020.
(93) Huang, L.; Liu, J.; Zhang, F.; Dontsov, E.; Damjanac, B. Exploring the influence of rock inherent heterogeneity and grain size on hydraulic fracturing using discrete element modeling. *International Journal of Solids and Structures* **2019**, *176*−*177*, 207−220.
(94) Dou, F.; Wang, J. G. A numerical investigation for the impacts of shale matrix heterogeneity on hydraulic fracturing with a two-dimensional particle assemblage simulation model. *Journal of Natural Gas Science and Engineering* **2022**, *104*, 104678.
(95) Wu, M.; Gao, K.; Liu, J.; Song, Z.; Huang, X. Influence of rock heterogeneity on hydraulic fracturing: A parametric study using the combined finite-discrete element method. *International Journal of Solids and Structures* **2022**, *234*−*235*, 111293.
(96) Wu, M.; Jiang, C.; Song, R.; Liu, J.; Li, M.; Liu, B.; Shi, D.; Zhu, Z.; Deng, B. Comparative study on hydraulic fracturing using different discrete fracture network modeling: Insight from homogeneous to heterogeneity reservoirs. *Engineering Fracture Mechanics* **2023**, *284*, 109274.
(97) Gao, Y.; Liu, H.; Pu, C.; Tang, H.; Yang, K.; Dong, X. Impact of geomechanical heterogeneity on multiple hydraulic fracture propagation. *Journal of Geophysics and Engineering* **2021**, *18* (6), 954−969.
(98) Wan, L.; Chen, M.; Hou, B.; Kao, J.; Zhang, K.; Fu, W. Experimental investigation of the effect of natural fracture size on hydraulic fracture propagation in 3D. *Journal of Structural Geology* **2018**, *116*, 1−11.
(99) Lin, H.; Li, D.; Jin, Q.; Guo, R.; Liu, J. Influences of natural cracks on fracturing. *Oil Geophysical Prospecting* **2018**, *53*, 156−161 + 167 +13.
(100) Shen, C.; Xie, J.; Zhao, J.; Fan, Y.; Ren, L. Whole-life cycle countermeasures to improve the stimulation effect of network fracturing in deep shale gas reservoirs of the Southern Sichuan Basin. *Natural Gas Industry* **2021**, *41*, 169−177.
(101) Wang, H. Hydraulic fracture propagation in naturally fractured reservoirs: Complex fracture or fracture networks. *Journal of Natural Gas Science and Engineering* **2019**, *68*, 102911.
(102) Yi, L.; Yang, C.; Yang, Z.; Song, Y.; He, X.; Zhou, X.; Li, X.; Hu, J. Influence of natural fracture zones on the propagation of hydraulic fractures in deep shale. *Natural Gas Industry* **2022**, *42*, 84−97.
(103) Dehghan, A. N. An experimental investigation into the influence of pre-existing natural fracture on the behavior and length of propagating hydraulic fracture. *Engineering Fracture Mechanics* **2020**, *240*, 107330.
(104) Liu, Y.; Zheng, X.; Peng, X.; Zhang, Y.; Chen, H.; He, J. Influence of natural fractures on propagation of hydraulic fractures in tight reservoirs during hydraulic fracturing. *Marine and Petroleum Geology* **2022**, *138*, 105505.
(105) Yao, Y.; Wang, W.; Keer, L. M. An energy based analytical method to predict the influence of natural fractures on hydraulic fracture propagation. *Engineering Fracture Mechanics* **2018**, *189*, 232−245.
(106) Zheng, H.; Pu, C.; Sun, C. Study on the interaction between hydraulic fracture and natural fracture based on extended finite element method. *Engineering Fracture Mechanics* **2020**, *230*, 106981.
(107) Liu, Z.; Pan, Z.; Li, S.; Zhang, L.; Wang, F.; Han, L.; Zhang, J.; Ma, Y.; Li, H.; Li, W. Study on the effect of cemented natural fractures on hydraulic fracture propagation in volcanic reservoirs. *Energy* **2022**, *241*, 122845.

https://doi.org/10.1021/acsomega.3c08547
ACS Omega 2024, 9, 117−136

(108) Wang, W.; Olson, J. E.; Prodanović, M.; Schultz, R. A. Interaction between cemented natural fractures and hydraulic fractures assessed by experiments and numerical simulations. *J. Pet. Sci. Eng.* **2018**, *167*, 506−516.
(109) Wang, H.; Li, G.; He, Z.; Shen, Z.; Li, X.; Zhang, Z.; Wang, M.; Yang, B.; Zheng, Y.; Shi, L. Analysis of mechanisms of supercritical CO_2 fracturing. *Rock and Soil Mechanics* **2018**, *39*, 3589−3596.
(110) Zhao, W.; Ji, G.; Li, K.; Liu, W.; Xiong, L.; Xiao, J. A new pseudo 3D hydraulic fracture propagation model for sandstone reservoirs considering fracture penetrating height. *Engineering Fracture Mechanics* **2022**, *264*, 108358.
(111) Liu, J.; Ding, W.; Xiao, Z.; Dai, J. Advances in comprehensive characterization and prediction of reservoir fractures. *Prog. Geophys.* **2019**, *34*, 2283−2300.
(112) Weng, X. Modeling of complex hydraulic fractures in naturally fractured formation. *Journal of Unconventional Oil and Gas Resources* **2015**, *9*, 114−135.
(113) Zheng, H.; Pu, C.; Sun, C. Numerical investigation on the hydraulic fracture propagation based on combined finite-discrete element method. *Journal of Structural Geology* **2020**, *130*, 103926.
(114) Wasantha, P. L. P.; Konietzky, H.; Weber, F. Geometric nature of hydraulic fracture propagation in naturally-fractured reservoirs. *Computers and Geotechnics* **2017**, *83*, 209−220.
(115) Wang, Y.; Hou, B.; Wang, D.; Jia, Z. Features of fracture height propagation in cross-layer fracturing of shale oil reservoirs. *Petroleum Exploration and Development* **2021**, *48* (2), 469−479.
(116) Memon, S.; Feng, R.; Ali, M.; Bhatti, M. A.; Giwelli, A.; Keshavarz, A.; Xie, Q.; Sarmadivaleh, M. Supercritical CO2-Shale interaction induced natural fracture closure: Implications for scCO2 hydraulic fracturing in shales. *Fuel* **2022**, *313*, 122682.
(117) Dwyer-Joyce, R. S.; Drinkwater, B. W.; Quinn, A. M. The Use of Ultrasound in the Investigation of Rough Surface Interfaces. *Journal of Tribology* **2001**, *123* (1), 8−16.
(118) Kartal, M. E.; Mulvihill, D. M.; Nowell, D.; Hills, D. A. Measurements of pressure and area dependent tangential contact stiffness between rough surfaces using digital image correlation. *Tribiol. Int.* **2011**, *44* (10), 1188−1198.
(119) Liu, Y.; Yang, H.; Zhang, Q.; Xiong, D. Properties of a shale bedding plane and its influence on the geometric parameters of fracture propagation in volume fracturing. *Engineering Fracture Mechanics* **2022**, *266*, 108413.
(120) Tan, P.; Pang, H.; Zhang, R.; Jin, Y.; Zhou, Y.; Kao, J.; Fan, M. Experimental investigation into hydraulic fracture geometry and proppant migration characteristics for southeastern Sichuan deep shale reservoirs. *J. Pet. Sci. Eng.* **2020**, *184*, 106517.
(121) Tan, P.; Jin, Y.; Han, K.; Hou, B.; Chen, M.; Guo, X.; Gao, J. Analysis of hydraulic fracture initiation and vertical propagation behavior in laminated shale formation. *Fuel* **2017**, *206*, 482−493.
(122) Wan, L.; Hou, B.; Tan, P.; Chang, Z.; Muhadasi, Y. Observing the effects of transition zone properties on fracture vertical propagation behavior for coal measure strata. *Journal of Structural Geology* **2019**, *126*, 69−82.
(123) Hou, B.; Cui, Z. Vertical fracture propagation behavior upon supercritical carbon dioxide fracturing of multiple layers. *Engineering Fracture Mechanics* **2023**, *277*, 108913.
(124) Liu, P.; Ju, Y.; Ranjith, P. G.; Zheng, Z.; Chen, J. Experimental investigation of the effects of heterogeneity and geostress difference on the 3D growth and distribution of hydrofracturing cracks in unconventional reservoir rocks. *Journal of Natural Gas Science and Engineering* **2016**, *35*, 541−554.
(125) Zhang, J.; Li, Y.; Pan, Y.; Wang, X.; Yan, M.; Shi, X.; Zhou, X.; Li, H. Experiments and analysis on the influence of multiple closed cemented natural fractures on hydraulic fracture propagation in a tight sandstone reservoir. *Engineering Geology* **2021**, *281*, 105981.
(126) Middleton, R.; Viswanathan, H.; Currier, R.; Gupta, R. CO2 as a fracturing fluid: Potential for commercial-scale shale gas production and CO2 sequestration. *Energy Procedia* **2014**, *63*, 7780−7784.
(127) Zhang, X.; Zhu, W.; Xu, Z.; Liu, S.; Wei, C. A review of experimental apparatus for supercritical CO2 fracturing of shale. *J. Pet. Sci. Eng.* **2022**, *208*, 109515.
(128) Zhao, Z.; Li, X.; He, J.; Mao, T.; Zheng, B.; Li, G. A laboratory investigation of fracture propagation induced by supercritical carbon dioxide fracturing in continental shale with interbeds. *J. Pet. Sci. Eng.* **2018**, *166*, 739−746.
(129) Gao, Q.; Han, S.; Cheng, Y.; Yan, C.; Sun, Y.; Han, Z. Effects of non-uniform pore pressure field on hydraulic fracture propagation behaviors. *Engineering Fracture Mechanics* **2019**, *221*, 106682.
(130) Ma, L.; Fauchille, A.-L.; Chandler, M. R.; Dowey, P.; Taylor, K. G.; Mecklenburgh, J.; Lee, P. D. In-situ synchrotron characterisation of fracture initiation and propagation in shales during indentation. *Energy* **2021**, *215*, 119161.
(131) Tao, J.; Meng, S.; Jin, X.; Xu, J.; Yang, Q.; Wang, X.; Liu, H.; Peng, B. Stimulation and Sequestration Mechanism of CO2 Waterless Fracturing for Continental Tight Oil Reservoirs. *ACS Omega* **2021**, *6* (32), 20758−20767.
(132) Nianyin, L.; Jiajie, Y.; Chao, W.; Suiwang, Z.; Xiangke, L.; Jia, K.; Yuan, W.; Yinhong, D. Fracturing technology with carbon dioxide: A review. *J. Pet. Sci. Eng.* **2021**, *205*, 108793.
(133) Zhang, Z.; Li, X.; He, J.; Wu, Y.; Li, G. Numerical study on the propagation of tensile and shear fracture network in naturally fractured shale reservoirs. *Journal of Natural Gas Science and Engineering* **2017**, *37*, 1−14.
(134) Jia, Y.; Lu, Y.; Elsworth, D.; Fang, Y.; Tang, J. Surface characteristics and permeability enhancement of shale fractures due to water and supercritical carbon dioxide fracturing. *J. Pet. Sci. Eng.* **2018**, *165*, 284−297.
(135) Estrada, J. M.; Bhamidimarri, R. A review of the issues and treatment options for wastewater from shale gas extraction by hydraulic fracturing. *Fuel* **2016**, *182*, 292−303.
(136) Luca, G. State of the art report on waterless stimulation techniques for shale formations, 2016.
(137) Akhondzadeh, H.; Keshavarz, A.; Awan, F. U. R.; Al-Yaseri, A. Z.; Iglauer, S.; Lebedev, M. Coal fracturing through liquid nitrogen treatment: a micro-computed tomography study. *APPEA Journal* **2020**, *60* (1), 67−76.
(138) Memon, K. R.; Mahesar, A. A.; Ali, M.; Tunio, A. H.; Mohanty, U. S.; Akhondzadeh, H.; Awan, F. U. R.; Iglauer, S.; Keshavarz, A. Influence of Cryogenic Liquid Nitrogen on Petro-Physical Characteristics of Mancos Shale: An Experimental Investigation. *Energy Fuels* **2020**, *34* (2), 2160−2168.
(139) Jiang, L.; Cheng, Y.; Han, Z.; Gao, Q.; Yan, C.; Wang, H.; Fu, L. Effect of liquid nitrogen cooling on the permeability and mechanical characteristics of anisotropic shale. *Journal of Petroleum Exploration and Production Technology* **2019**, *9* (1), 111−124.
(140) Moridis, G. J. Literature Review and Analysis of Waterless Fracturing Methods, 2018.
(141) Zhou, D.; Zheng, P.; Yang, J.; Li, M.; Xia, Y.; Cai, W.; Ma, X.; Liu, S. Optimizing the construction parameters of modified zipper fracs in multiple horizontal wells. *Journal of Natural Gas Science and Engineering* **2019**, *71*, 102966.
(142) Li, C.; Liang, W.; Hou, D.; Yao, H.; Song, X. Comparison of Fracturing Features and Permeability Enhancement of Coal Fractured by Water and Supercritical CO_2. *Journal of Taiyuan University of Technology* **2019**, *50*, 485−491.
(143) Liu, G.; Xian, X.; Zhou, J.; Zhang, L.; Liu, Q.; Zhao, Y.; Zhang, S. Experimental study on the supercritical CO_2 fracturing of shale. *Journal of China Coal Society* **2017**, *42*, 694−701.
(144) Ma, D.; Cheng, C.; Ding, C.; Song, J.; Hu, D.; Zhou, H. Comparisons of fracturing mechanism of tight sandstone using liquid CO2 and water. *Journal of Natural Gas Science and Engineering* **2021**, *94*, 104108.
(145) Guo, T.; Tang, S.; Liu, S.; Liu, X.; Zhang, W.; Qu, G. Numerical simulation of hydraulic fracturing of hot dry rock under thermal stress. *Engineering Fracture Mechanics* **2020**, *240*, 107350.

https://doi.org/10.1021/acsomega.3c08547
ACS Omega 2024, 9, 117−136

(146) Wang, L. Study on the influence of temperature on fracture propagation in ultra-deep shale formation. *Engineering Fracture Mechanics* **2023**, *281*, 109118.
(147) Zhang, L.; Mao, X.; Liu, R.; Guo, X.; Ma, D. The Mechanical Properties of Mudstone at High Temperatures: an Experimental Study. *Rock Mechanics and Rock Engineering* **2014**, *47* (4), 1479−1484.
(148) Du, D.; Liu, P.; Teng, J.; Zhang, Z.; Li, Y.; Tang, Y.; Li, X.; Zhao, Y. Numerical Simulation of Multicrack Propagation Dynamics in Supercritical CO2 Fracturing of Tight Reservoirs. *Energy Fuels* **2022**, *36* (22), 13526−13539.
(149) Gupta, D. V. S.; Bobier, D. M. *The History and Success of Liquid CO2 and CO2/N2 Fracturing System*; SPE Gas Technology Symposium, 1998.
(150) Jing, X.; Wang, Z.; Zhang, Q.; Yu, Z.; Li, C.; Huang, J.; Fang, Y. Evaluation of CO2 Gasification Reactivity of Different Coal Rank Chars by Physicochemical Properties. *Energy Fuels* **2013**, *27* (12), 7287−7293.
(151) Yan, H.; Zhang, J.; Zhou, N.; Li, M.; Suo, Y. Numerical simulation of dynamic interactions between two cracks originating from adjacent boreholes in the opposite directions during supercritical CO2 fracturing coal mass. *Engineering Fracture Mechanics* **2020**, *223*, 106745.
(152) Jiang, T. Discussion on Several Key Issues of the New-Generation Network Fracturing Technologies for Unconventional Reservoirs. *Petroleum Drilling Techniques* **2023**, *51*, 184−191.
(153) Li, Y.; Hu, W.; Zhang, Z.; Zhang, Z.; Shang, Y.; Han, L.; Wei, S. Numerical simulation of hydraulic fracturing process in a naturally fractured reservoir based on a discrete fracture network model. *Journal of Structural Geology* **2021**, *147*, 104331.
(154) Yang, F.; Mei, W.; Li, L.; Sun, Z.; An, Q.; Yang, Q.; Lu, M.; Yang, R. Propagation of hydraulic fractures in thin interbedded tight sandstones. *Coal Geol. Exploration* **2023**, *51*, 61−71.
(155) Perkins, T. K.; Kern, L. R. Widths of Hydraulic Fractures. *Journal of Petroleum Technology* **1961**, *13* (09), 937−949.
(156) Nordgren, R. P. Propagation of a Vertical Hydraulic Fracture. *Society of Petroleum Engineers Journal* **1970**, *12* (04), 306−314.
(157) Geertsma, J.; De Klerk, F. A Rapid Method of Predicting Width and Extent of Hydraulically Induced Fractures. *Journal of Petroleum Technology* **1969**, *21* (12), 1571−1581.
(158) Khristianovich, S. A.; Zheltov, Y. P. Formation of Vertical Fractures by Means of Highly Viscous Liquid, 1955.
(159) Li, Q.; Li, T.; Cai, Y.; Liu, D.; Li, L.; Ru, Z.; Yin, T. Research progress on hydraulic fracture characteristics and controlling factors of coalbed methane reservoirs. *Journal of China Coal Society* **2023**, 1−19.
(160) Settari, A.; Cleary, M. P. Development and Testing of a Pseudo-Three-Dimensional Model of Hydraulic Fracture Geometry. *SPE Production Engineering* **1986**, *1* (06), 449−466.
(161) Kresse, O.; Weng, X.; Gu, H.; Wu, R. Numerical Modeling of Hydraulic Fractures Interaction in Complex Naturally Fractured Formations. *Rock Mechanics and Rock Engineering* **2013**, *46* (3), 555−568.
(162) Chuprakov, D.; Melchaeva, O.; Prioul, R. *Injection-Sensitive Mechanics of Hydraulic Fracture Interaction with Discontinuities*; 47th US Rock Mechanics/Geomechanics Symposium, 2013.
(163) Ma, X.; Zou, Y.; Li, N.; Chen, M.; Zhang, Y.; Liu, Z. Experimental study on the mechanism of hydraulic fracture growth in a glutenite reservoir. *Journal of Structural Geology* **2017**, *97*, 37−47.
(164) Yin, H.; Zhou, J.; Xian, X.; Jiang, Y.; Lu, Z.; Tan, J.; Liu, G. Experimental study of the effects of sub- and super-critical CO2 saturation on the mechanical characteristics of organic-rich shales. *Energy* **2017**, *132*, 84−95.
(165) Wu, M.; Wang, W.; Song, Z.; Liu, B.; Feng, C. Exploring the influence of heterogeneity on hydraulic fracturing based on the combined finite-discrete method. *Engineering Fracture Mechanics* **2021**, *252*, 107835.
(166) Munjiza, A.; Owen, D. R. J.; Bicanic, N. A combined finite-discrete element method in transient dynamics of fracturing solids. *Engineering Computations* **1995**, *12* (2), 145−174.
(167) Deng, P.; Liu, Q.; Huang, X.; Bo, Y.; Liu, Q.; Li, W. Sensitivity analysis of fracture energies for the combined finite-discrete element method (FDEM). *Engineering Fracture Mechanics* **2021**, *251*, 107793.
(168) Ding, H.; Fu, X.; Sheng, Q.; Chen, J.; Yan, C.; Tian, K.; Hu, B. Study on Macroscopic Mechanical Behavior and Meso-failure Evolution of Gabbro of Different Particle Sizes. *Rock Mechanics and Rock Engineering* **2023**, *56*, 8947.
(169) Luo, Z.; Yan, C.; Ke, W.; Wang, T.; Xiao, M. A surrogate model based on deep convolutional neural networks for solving deformation caused by moisture diffusion. *Engineering Analysis with Boundary Elements* **2023**, *157*, 353−373.
(170) Wu, L.; Hou, Z.; Luo, Z.; Xiong, Y.; Zhang, N.; Luo, J.; Fang, Y.; Chen, Q.; Wu, X. Numerical simulations of supercritical carbon dioxide fracturing: A review. *Journal of Rock Mechanics and Geotechnical Engineering* **2023**, *15* (7), 1895−1910.
(171) Feng, W.; Were, P.; Li, M.; Hou, Z.; Zhou, L. Numerical study on hydraulic fracturing in tight gas formation in consideration of thermal effects and THM coupled processes. *J. Pet. Sci. Eng.* **2016**, *146*, 241−254.
(172) Lisjak, A.; Grasselli, G. A review of discrete modeling techniques for fracturing processes in discontinuous rock masses. *Journal of Rock Mechanics and Geotechnical Engineering* **2014**, *6* (4), 301−314.
(173) Sharafisafa, M.; Aliabadian, Z.; Sato, A.; Shen, L. Coupled Thermo-hydro-mechanical Simulation of Hydraulic Fracturing in Deep Reservoirs Using Finite-Discrete Element Method. *Rock Mechanics and Rock Engineering* **2023**, *56* (7), 5039−5075.

https://doi.org/10.1021/acsomega.3c08547
ACS Omega 2024, 9, 117−136